Manuscript (non-LaTeX)

Effects of Scale-Aware Convection Schemes on Typhoon Simulation across Varying Resolutions

Yanjie Liu[1, 2], Xiaocong Wang[3], Yimin Liu[1, 2], Hao Miao[4, 5], Dajun Zhao[6], Wei Huang[7], Xuesong Zhu[7], Yaxin Zhao[1, 2]

1. *State Key Laboratory of Earth System Numerical Modeling and Application, Institute of Atmospheric Physics, Chinese Academy of Sciences, Beijing, China*
2. *College of Earth and Planetary Sciences, University of Chinese Academy of Sciences (UCAS), Beijing, China*
3. *Institute of Atmospheric Physics (IAP), Chinese Academy of Sciences (CAS), Beijing, China*
4. *Nanjing Innovation Institute for Atmospheric Sciences, Chinese Academy of Meteorological Sciences–Jiangsu Meteorological Service, Nanjing, China*
5. *Jiangsu Key Laboratory of Severe Storm Disaster Risk / Key Laboratory of Transportation Meteorology of CMA, Nanjing, China*
6. *State Key Laboratory of Severe Weather Meteorological Science and Technology, Chinese Academy of Meteorological Sciences, Beijing, China*
7. *Shanghai Typhoon Institute, China Meteorological Administration, Shanghai, China*

Submitted to *Monthly Weather Review (revised)*

Corresponding author: Xiaocong Wang, wangxc@lasg.iap.ac.cn; Yimin Liu, lym@lasg.iap.ac.cn

Early Online Release: This preliminary version has been accepted for publication in *Monthly Weather Review*, may be fully cited, and has been assigned DOI 10.1175/MWR-D-25-0241.1. The final typeset copyedited article will replace the EOR at the above DOI when it is published.

© 2026 American Meteorological Society. This is an Author Accepted Manuscript distributed under the terms of the default AMS reuse license. For information regarding reuse and general copyright information, consult the AMS Copyright Policy (www.ametsoc.org/PUBSReuseLicenses).

ABSTRACT

Through a suite of global simulations using the Global-to-Regional Integrated forecast SysTem (GRIST) model, this study investigates the impact of different scale-aware convective parameterization schemes (CPS) on typhoon simulation across resolutions from 60 to 3.75 km. Three implementations are examined: scaling convective adjustment time (CTRL), scaling cloud-base mass flux (SA-MB), and scaling entrainment rate (SA-ER). All CPS show improved performance with increasing resolution. CTRL and SA-MB exhibit comparable scale-adaptivity, whereas SA-ER demonstrates stronger CPS suppression and outperforms the other two, reducing mean track errors by 10–45 km and intensity underestimation by 8–47%.

Decomposition of the surface pressure tendency budget reveals that SA-ER enhances microphysical processes more vigorously, more than offsetting the reduction of convective component and yielding a net ~10% increase in precipitation and diabatic heating, thereby deepening the storm. These benefits hold across most resolutions but diminish at the convection-permitting scale for typhoons that are not sufficiently compact and intense, where excessive outer-rainband warming disrupts the secondary circulation and weakens intensification. Explicit convection without CPS also performs poor at this resolution, producing the largest track and intensity errors among all experiments—underscoring that even at convection-permitting scales, scale-aware CPS remains indispensable. The results of this study demonstrate the advantages of scale-aware CPS on typhoon modeling, with the entrainment scaling approach emerging as a particularly effective pathway for improving typhoon intensity forecasts.

SIGNIFICANCE STATEMENT

Typhoons are among the most devastating weather systems, posing severe threats to human life and economies. Accurately simulation of typhoon intensity remains a great challenge, as tropical cyclones involve complex multiscale interactions between

Accepted for publication in *Monthly Weather Review.* DOI 10.1175/MWR-D-25-0241.1.

cumulus convection and large-scale dynamics. By examining the impact of different scale-aware convective parameterization schemes on typhoon simulations and elucidating the mechanisms through which convection schemes affect typhoon intensity, this study offers an effective pathway toward improving typhoon intensity forecasts and optimizing convective parameterization in numerical models.

1. Introduction

Typhoons are among the most devastating weather systems that threaten lives, infrastructure, and economies across vast coastal and inland regions. Their destructive potential creates an urgent societal demand for accurate forecasts, yet they continue to pose persistent challenges for numerical weather prediction (NWP) models despite that substantial progress has been made in typhoon track prediction over the past decades (Peng et al. 2017; Landsea and Cangialosi 2018; Lei et al. 2022). The reliable simulation of typhoon intensity, particularly during rapid intensification, remains a formidable challenge owing to the complex multiscale interactions within typhoon systems (Rogers et al. 2015; Tan et al. 2022). Current NWP models have a long-standing tendency to underestimate typhoon intensity, especially for intense storms, as documented in numerous studies (e.g., Yu et al. 2013; Shi et al. 2025). Similar underestimation issues are also evident in hindcast experiments (e.g., Jin et al. 2014; Meng et al. 2024), suggesting that the challenge is not only real-time forecast skill but also intrinsic model limitations in representing the physics of typhoon intensification (Emanuel 2018). The challenge arises because tropical cyclones involve multiscale interactions between cumulus convection and large-scale dynamics, spanning a broad spectrum of spatial and temporal scales (Gu et al. 2015; Rios-Berrios et al. 2018; Li and Dai 2020). Accurately capturing these interactions is particularly difficult, as small-scale convective processes strongly modulate the evolution of the larger-scale circulation, and vice versa. This renders typhoon forecast highly sensitive to model resolution and the representation of convection, which is well documented in the

Accepted for publication in *Monthly Weather Review.* DOI 10.1175/MWR-D-25-0241.1.

literature (Gentry and Lackmann 2010; Judt et al. 2021; Polichtchouk et al. 2025). Therefore, a proper representation of convection and its feedback on the surrounding environment at finer resolutions remain a cornerstone for advancing TC forecasting (Vitart et al. 2001; Tan et al. 2022).

Traditionally, cumulus convection in general circulation models (GCMs) is represented by convective parameterization schemes (CPS), in which convection is treated as a subgrid-scale process. As model resolution approaches tens of kilometer scale, the validity of CPS becomes questionable because some organized convection can be resolved and convection is no longer a pure subgrid-scale phenomenon (Molinari & Dudek, 1992; Arakawa & Wu, 2013; Song & Zhang, 2018). Within this "gray zone" where convection is partially resolved by model dynamics, the contribution of CPS should gradually diminish as grid spacing decreases (Hong and Dudhia 2012). This concept forms the basis of scale-aware CPS, in which resolution-dependent scaling factors are introduced to ensure that subgrid-scale convective eddy transports vanish in the limit of grid spacing approaching zero (Wang 2022). On the other hand, some studies opted to switch off CPS at convection-permitting scales, which was found to improve the representation of mesoscale convective systems (Weisman et al. 1997; Knippertz et al. 2009). However, this strategy often renders under-resolved circulations overly energetic, leading to systematic forecast problems such as delayed convection onset and overprediction of heavy rainfall (Weisman et al. 1997; Bryan and Morrison 2012). To address this challenge, several scale-aware modifications to CPS have been proposed, including approaches such as scaling mass flux by convective cloud fraction (Arakawa and Wu 2013; Grell and Freitas 2014), lengthening convective adjustment timescales with grid resolution (Zheng et al. 2016; Wang 2022), and scaling entrainment rates as a function of resolution (Zheng et al. 2016; Zhao et al. 2024).

While the influence of scale-aware CPS on general model performance has been extensively studied (Ahn and Kang 2018; Freitas et al. 2020; Park et al. 2024), relatively

Accepted for publication in *Monthly Weather Review.* DOI 10.1175/MWR-D-25-0241.1.

few have focused specifically on their impacts on tropical cyclones (Wang 2022; Liu et al. 2025). By conducting typhoon simulations with different scale-aware CPS and comparing them against a default CPS, this study aims to address three central questions: (i) What are the differences among various scale-aware CPS in typhoon modeling, and how does their performance vary with resolution? (ii) To what extent and through what mechanisms do scale-aware CPS improve typhoon simulations? (iii) Can scale-aware CPS outperform explicit simulations at the convection-permitting scale? Addressing these questions will advance our understanding of the role of CPS in model performance and provide guidance for improving typhoon forecasts. The remainder of this paper is structured as follows. Section 2 describes the model, the formulations of scale-aware CPS, and the experimental design, followed by an evaluation of the scale adaptivity of each CPS in Section 3. Section 4 investigates the impacts of different scale-aware CPS on typhoon simulations using Typhoon Lekima (2019) as a case study, with additional verification based on Typhoon Soudelor (2015) in Section 5. Finally, Section 6 provides conclusions and discussion.

2. Model Description and Experimental Design

a. Model Description and scale-aware CPS formulations

To investigate the impact of scale-aware CPS on typhoon modeling across different resolutions, we use the Global-to-Regional Integrated forecast SysTem (GRIST; Zhang et al. 2019, 2021; Li et al. 2022) model, which solves the fully compressible Euler equations, with vertical acceleration retained for nonhydrostatic dynamics (Zhang et al. 2019). For physics packages, the model includes the Yonsei University (YSU) scheme for boundary layer turbulence (Hong et al. 2006), the WRF single moment six-class (WSM6) scheme for cloud microphysics (Hong and Lim, 2006), and the Rapid Radiative Transfer Model for GCM Applications (RRTMG; Iacono et al. 2008). Regarding convection, GRIST uses a bulk mass-flux scheme originally proposed by Tiedtke (TDK; 1989), with subsequent modifications by Bechtold et al. (2008, 2014).

Accepted for publication in *Monthly Weather Review.* DOI 10.1175/MWR-D-25-0241.1.

The coding and implementation are based on Zhang and Wang (2017). Theses updates introduce a scaling factor in terms of grid-size Δx for convective adjustment time τ, which acts to reduce convection with increasing resolution and is expressed below:

$$\tau = \begin{cases} \dfrac{H}{\overline{w}_{up}}\left(1 + 1.6\dfrac{\Delta x}{125}\right) & \Delta x \geq 8\ km \\ \dfrac{H}{\overline{w}_{up}}\left(1 + \left(\ln\left(\dfrac{10}{\Delta x}\right)\right)^2\right) & \Delta x < 8\ km \end{cases} \quad (1)$$

where H is the cloud depth, and $\overline{w}_{up}$ is the averaged updraft velocity within cloud. Based on this scheme, two alternative scale-aware implementations were introduced. The first method (SA-MB) scales cloud-base mass flux using the convective fraction σ, following Arakawa and Wu (2013), it is expressed as:

$$M_b = (1 - \sigma)^2 M_b^* \quad (2)$$

where M_b stands for the cloud-base cumulus mass flux and M_b^* the equilibrium M_b required for full adjustment responding to the grid-scale destabilization. We found the convective fraction σ calculated according to Arakawa and Wu (2013) tends to be unrealistically small, even at a resolution of 3.75 km. We therefore adopt the formulation of Grell and Freitas (2014), in which σ is calculated as:

$$\sigma = \frac{\pi R_c^2}{A_{grid}} \quad (3)$$

In Eq. (3), A_{grid} denotes the grid-box area, and R_c the radius of the convective updraft, which is related to the entrainment rate ε_b at cloud base by $R_c = \frac{0.2}{\varepsilon_b}$.

Another approach is to increase the entrainment rate, motivated by studies demonstrating its resolution dependence (e.g., Stevens and Bretherton 1999; Romps and Kuang 2010; Bryan and Morrison 2012). Based on these findings, modifying the entrainment rate to achieve scale-awareness has been proposed (Zheng et al. 2016), and has shown good performance in suppressing spurious convection and improving precipitation forecasts at high resolutions (Lim et al. 2015; Park et al. 2022). The second method (SA-ER) achieves scale awareness by scaling the entrainment rate ε of Bechtold et al. (2008) following the empirical power-law relationship proposed by Zhao

Accepted for publication in *Monthly Weather Review.* DOI 10.1175/MWR-D-25-0241.1.

et al. (2024) based on LES diagnosis. In this formulation, ε depends on both environmental relative humidity (RH) and horizontal grid spacing Δx (km) calculated as the square root of the grid cell area, written as:

$$\varepsilon = \varepsilon_0(1.3 - RH)\left(\frac{q_{sat}(\bar{T})}{q_{sat}(\bar{T}_{base})}\right)^3\left(\frac{L}{\Delta x}\right)^{0.2} \quad (4)$$

where ε_0 is an empirical mixing rate that distinguishes between shallow and deep convection, q_{sat} is for saturated specific humidity, and L is a reference horizontal scale of 256 km following Zhao et al. (2024), representing the typical horizontal scale at coarse resolutions. As resolution refines to 3.75 km, SA-ER increases the entrainment rate by approximately 2.33 times relative to CTRL, which effectively suppresses parameterized deep convection while promoting shallow convection. Consequently, SA-ER introduces an intensified cold bias in the mid-to-upper troposphere but alleviates the cold bias near 600 hPa compared to CTRL; it also exhibits a more pronounced moist bias at 900 hPa while reducing the moist bias above 850 hPa (Figure S1). These thermodynamic adjustments enhance vertical conditional instability, thereby creating more favorable conditions for resolved-scale microphysics to take over energy release.

b. Experimental Design

We selected two typhoon cases: Lekima (2019) and Soudelor (2015), which are among the most powerful and catastrophic storms of their respective years, to explore the impact of scale-aware CPS on typhoon modeling. Three groups of experiments were conducted using quasi-uniform grids for global simulations: a control simulation using the original CPS (CTRL), a simulation using the scale-aware cloud-base mass flux scheme (SA-MB), and another using the scale-aware entrainment scheme (SA-ER). Each group consisted of five simulations with different horizontal resolutions, *i.e.,* 60 km, 30 km, 15 km, 7.5 km and 3.75 km. In addition, a convection-permitting simulation without CPS (NOCP) at 3.75-km resolution was also performed. All experiments were

Accepted for publication in *Monthly Weather Review.* DOI 10.1175/MWR-D-25-0241.1.

initialized with ERA5 reanalysis (Hersbach et al. 2020) at 0.25° spatial resolution, using conservative interpolation onto each model grid. The simulations were integrated for 72 h, focusing on the developing stage of the typhoons, for Lekima, from 0000 UTC 6 to 0000 UTC 9 August 2019; for Soudelor, from 1800 UTC 1 to 1800 UTC 4 August 2015. No specialized vortex initialization or bogus technique was applied during the initialization process. It is worth noting that, when initializing from a 0.25° reanalysis, the spin-up of tropical cyclones in the forecasts may be relatively slow. However, given that our analysis focuses on the period after the first 18 hours of integration, by which time the model physics has largely adjusted to the resolved dynamics, we consider the current experimental setup to be adequate.

3. Assessment of scale-adaptivity of CPS

Before exploring the performance of different CPS on typhoon simulations, we first explore how parameterized convective activity (often measured in terms of subgrid precipitation produced by CPS) responds to model resolution with different scale-aware implementations.

Figure 1 compares the total precipitation from the three groups of experiment at varying resolutions against Global Precipitation Measurement (GPM; Huffman et al. 2023). All simulations show close agreement with the observation, with global means ranging from 3.01 to 3.15 mm d^{-1}, compared to 2.97 mm d^{-1} in GPM. While total precipitation exhibits little sensitivity to resolution and convection scheme, the parameterized convective precipitation displays distinct resolution-dependent behaviors across the three experiments, as shown in Figure 2. In the CTRL runs (left column), strong CPS precipitation exceeding 10 mm d^{-1} is concentrated in the tropics, whereas weaker CPS precipitation less than 5 mm d^{-1} is mainly distributed in the midlatitudes. As resolution increases, convective precipitation gradually decreases, with the global mean reduced from 2.22 mm d^{-1} at 60 km to 1.74 mm d^{-1} at 3.75 km, indicating inherent scale-

Accepted for publication in *Monthly Weather Review.* DOI 10.1175/MWR-D-25-0241.1.

awareness in the default CPS scheme. A similar decreasing trend is also evident in SA-MB runs, and the reduction is more pronounced at 7.5- and 3.75-km resolutions, where the global mean drops to 1.96 and 1.44 mm d^{-1}, respectively. In SA-ER runs, CPS precipitation decreases more substantially with increasing resolution, declining to 1.73 mm d^{-1} at 7.5 km and 1.25 mm d^{-1} at 3.75 km, reflecting a stronger inhibition of parameterized convection compared to the other two.

To better quantify the variations described above and assess whether they behave similarly in the typhoon system, Figure 3 presents the ratio of CPS precipitation to total precipitation at different resolutions, both globally and within the typhoon system. The global ratio (Figure 3a) demonstrates a clearly decreasing trend with increasing resolution and a progressive enhancement of subgrid convective inhibition from CTRL to SA-MB and to SA-ER, starting from ~73% at 60 km and decreasing to 57%, 47%, and 40% at 3.75 km, respectively. This decline is consistent with the reduction of cloud-base cumulus mass flux shown in Figure 3c. Freitas et al., (2020) reported that their scale-aware convection scheme reduces the global CPR from 65% to 33% as resolution increases from 50 km to 3 km, a value even lower than the CPR of SA-ER. However, in terms of the reduction in CPR with increasing resolution, SA-ER shows a decrease of approximately 32%, identical to that reported in Freitas et al. (2020).

The ratio within the typhoon system, defined by a 600-km radius, exhibits a similar variation curve (Figure 3b) but with systematically higher values that reach ~85% at 60 km. The ratio then decreases more sharply than in the global mean, dropping to 22–45% at 3.75 km, as the highly organized convection in typhoons becomes increasingly explicitly resolved at finer resolutions. Note the difference between CTRL and SA-MB is indistinguishable. This occurs because σ, calculated according to Eq. (3), tends to be smaller over oceans than over land (thus greater scaling factor in Figure 3d, dotted line), owning to stronger cloud-base entrainment ε_b associated with lower cloud-base height in the former. For SA-ER, the transition between parameterized and explicitly resolved

Accepted for publication in *Monthly Weather Review.* DOI 10.1175/MWR-D-25-0241.1.

convection is non-trivial and strongly dependent on environmental relative humidity, proceeding more readily in moisture-abundant environments, such as within tropical cyclones, than under general conditions. The discrepancy between the global ratio and that in the typhoon system underscores the fact that scale-aware CPS exerts distinct impacts on typhoon simulation compared to its influence on the global mean state.

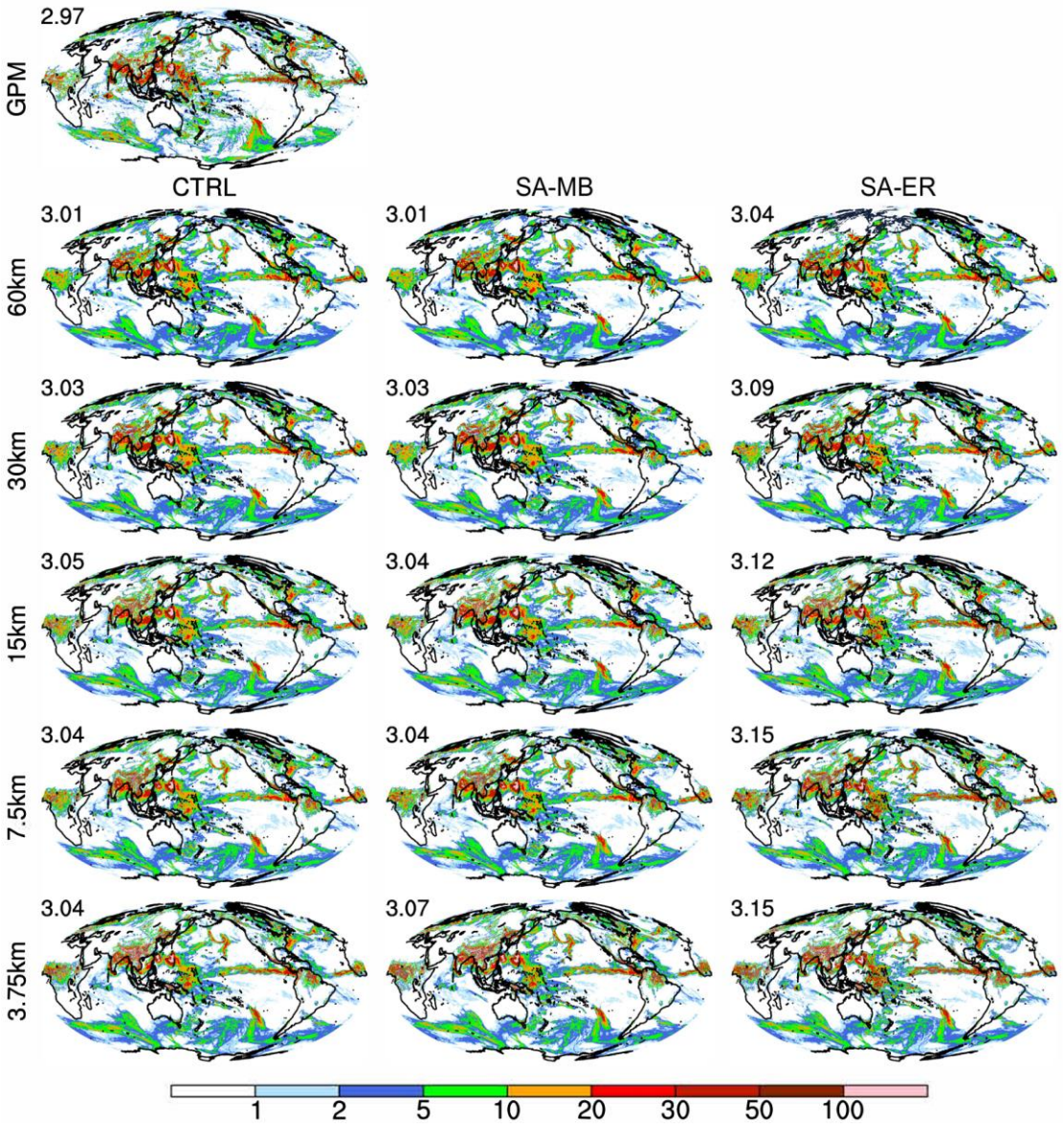


Figure 1 Spatial pattens of 72-h averaged total precipitation (mm d^{-1}) from GPM observation and experiments of CTRL (left), SA-MB (middle) and SA-ER (right) at different resolutions, with the global mean given in the top-left corner of each panel.

Accepted for publication in *Monthly Weather Review.* DOI 10.1175/MWR-D-25-0241.1.

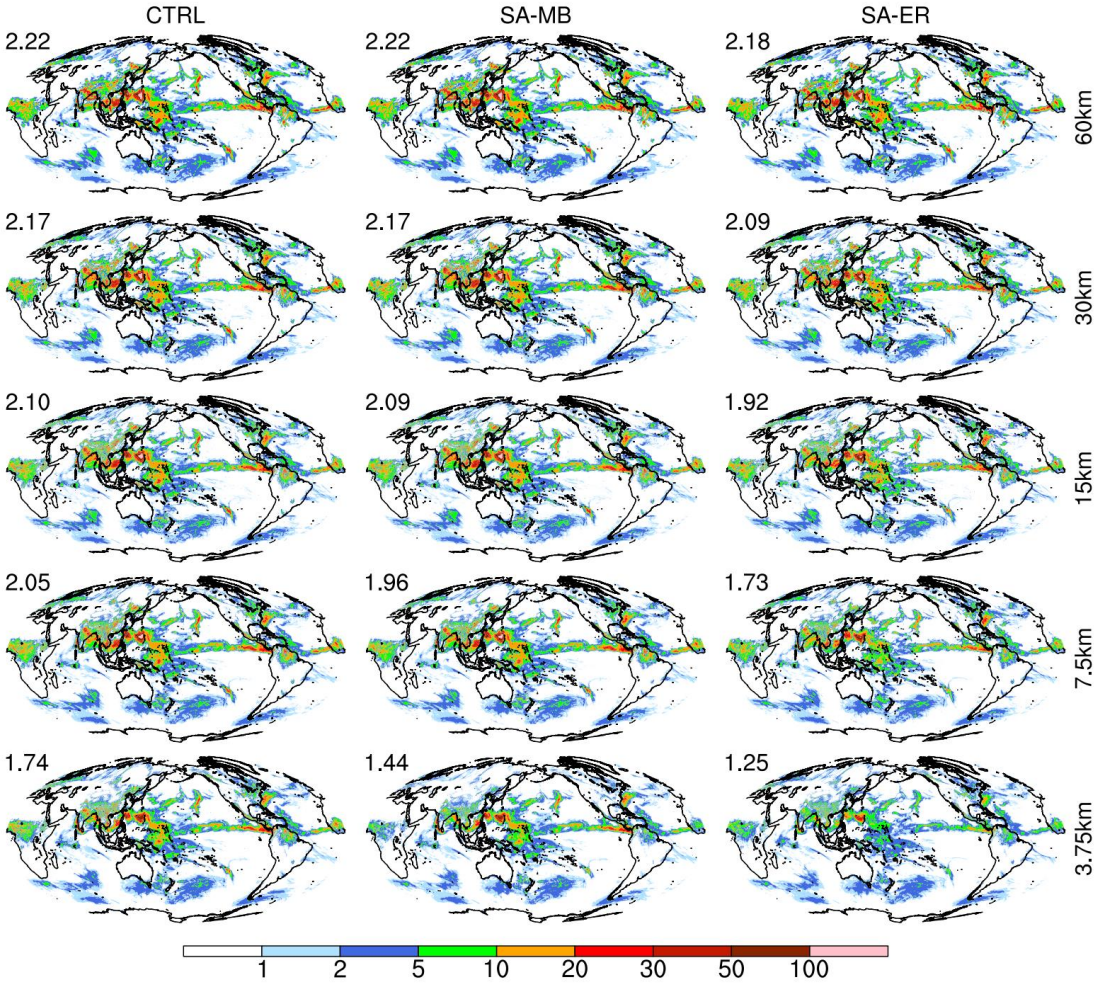


Figure 2 Spatial pattens of 72-h averaged precipitation (mm d−1) from convection parameterization schemes (CPS): CTRL (left), SA-MB (middle) and SA-ER (right) at different resolutions. Numbers on the top-left corner of each panel represent the global mean.

Accepted for publication in *Monthly Weather Review.* DOI 10.1175/MWR-D-25-0241.1.

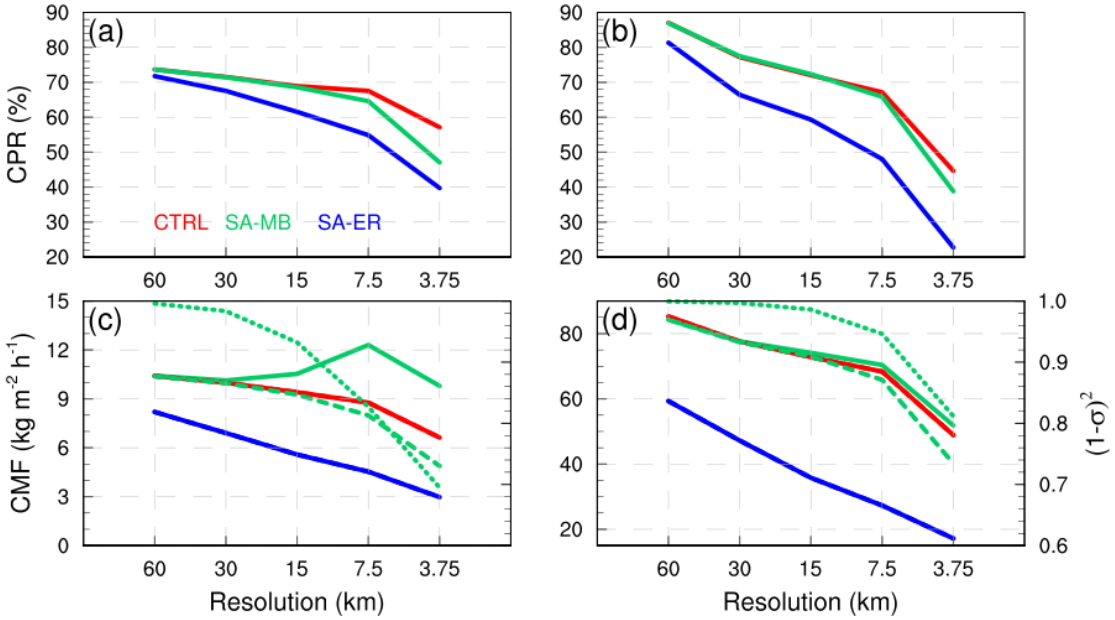


Figure 3 (a, b) Ratio of CPS precipitation to total precipitation (CPR), and (c, d) cloud-base cumulus mass flux M_b over (a, c) the globe and (b, d) the typhoon system within a 600-km radius. Dotted and dashed green lines in (c, d) represent the scaling factor $(1-\sigma)^2$ and the scaled M_b in SA-MB, respectively.

4. Impact of scale-aware CPS on typhoon simulation

a. Track and Intensity

Figure 4 presents the evolution of the track and intensity of typhoon Lekima over a 72-h period, as simulated with different CPS at varying resolutions. The best track data provided by the China Meteorological Administration (Lu et al. 2021) is also superimposed. The typhoon intensity is measured by the minimum sea-level pressure (p_{min}) and the maximum 10-m wind speed (v_{max}). According to the observation, Lekima moved northwestward and intensified into a typhoon by 1800 UTC 6 August. It then underwent rapid intensification accompanied by a northward deflection, ultimately reaching peak intensity at 1200 UTC 8 August, with p_{min}= 915 hPa and v_{max}= 62 m s^{-1}. Except for the 60-km runs, simulations at all other resolutions successfully capture the track during the first 36 h, with errors mostly within 60 km, whereas the 60-km simulations show substantial initial track errors. Beyond this period, the simulated tracks tend to deviate southwestward, as models fail to capture the

Accepted for publication in *Monthly Weather Review.* DOI 10.1175/MWR-D-25-0241.1.

observed northward deflection—a deficiency also common in operational forecast models (Huang et al. 2022). However, this bias is progressively reduced as resolution increases in all three simulations. At 3.75-km resolution, all simulations successfully reproduce the northward deflection, albeit with a slightly slower system movement compared to observations.

The CTRL and SA-MB tracks are nearly indistinguishable, whereas SA-ER produces a consistent northward shift across all resolutions, effectively reducing the mean position error by 15–45 km. The track improvement of SA-ER is presumably attributable to a more realistic simulation of the large-scale systems surrounding the typhoon—specifically, the position of Typhoon Krosa and the intensity of the western Pacific subtropical high (WPSH). As shown in Figure S2, compared to ERA5 reanalysis, the CTRL run tends to simulate Krosa too far northwest. This enhances the pressure gradient between Krosa and WPSH, resulting in stronger easterly winds that push Lekima farther west. In contrast, SA-ER shifts Krosa southeastward and strengthens the WPSH ridge between Lekima and Krosa, which intensifies southerly winds, and facilitates more northward motion of Lekima. Similar phenomenon is also found in Zhao et al. (2025).

Differences among the three experiments are evident in typhoon intensity as well. At 60-km resolution, SA-MB and CTRL yield nearly identical evolutions of p_{min} and v_{max}, both peaking at 960 hPa and 32 m s^{-1}. In contrast, SA-ER produces relatively stronger intensity, reducing the underestimation by approximately 5 hPa and 2 m s^{-1}. This enhanced intensity in SA-ER experiment persists at resolutions ranging from 30 km down to 7.5 km. At 3.75-km resolution, however, SA-ER yields the weakest typhoon among the three experiments, whereas CTRL and SA-MB exhibit intensity evolution most consistent with observations. Overall, SA-MB yields result largely consistent with CTRL, whereas SA-ER demonstrates better performance across all resolutions except at 3.75 km, yielding track improvements of 15–45 km and intensity

Accepted for publication in *Monthly Weather Review.* DOI 10.1175/MWR-D-25-0241.1.

enhancements of 10–39% on average.

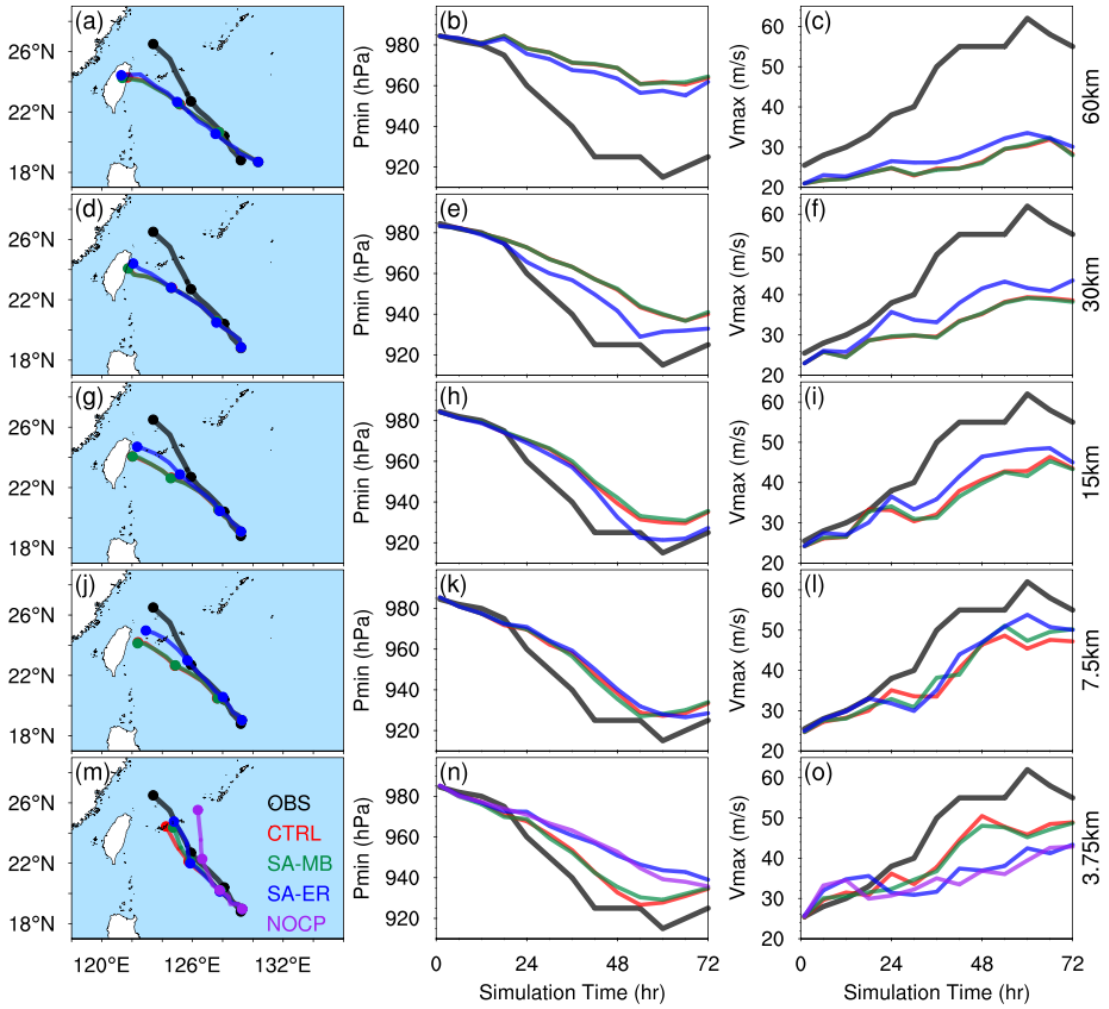


Figure 4 Observed and simulated 72-h (a, d, g, j, m) tracks, (b, e, h, k, n) minimum sea level pressure (p_{min}, hPa), and (c, f, i, l, o) maximum 10-m wind speed (v_{max}, m s^{-1}) for typhoon Lekima at resolutions of (a–c) 60 km, (d–f) 30 km, (g–i) 15 km, (j–l) 7.5 km, and (m–o) 3.75 km. Dots in (a, d, g, j, m) mark the typhoon locations at 24-h intervals.

b. Mechanisms of Typhoon Intensity: Diagnostics from Minimum Sea-Level Pressure

To understand how different scale-aware CPS influence typhoon intensity in terms of p_{min}, we applied the surface pressure tendency (SPT) equation introduced by Zhang & Ma (2023) to decompose the contributions from individual physical processes. The SPT equation is expressed as:

$$\underbrace{\frac{\partial p_s}{\partial t}}_{PS} = \underbrace{\frac{c_p}{R} {p_0}^{R/c_p} {p_s}^{1-R/c_p} \frac{\partial \pi_t}{\partial t}}_{PT} - \underbrace{\frac{g}{R} {p_0}^{R/c_p} {p_s}^{1-R/c_p} \int_{z_s}^{z_t} \frac{1}{\theta^2} \frac{\partial \theta}{\partial t} dz}_{THEN} \quad (5)$$

Accepted for publication in *Monthly Weather Review*. DOI 10.1175/MWR-D-25-0241.1.

where $\pi_t \equiv (p/p_0)^{R/c_p}$, z_s denotes the surface, z_t represents the top of the atmosphere, which is set to 20 km in this study. Other symbols follow conventional meteorological notations. Equation (5) indicates that the surface pressure change (PS) arises from two components: the pressure tendency at the upper boundary (PT) and the vertically integrated potential temperature tendency (THEN). Figure S3 presents the period-mean azimuthally averaged SPT terms, indicating that the THEN term dominates the radial distribution of PS, whereas the contribution from PT is negligible. This justifies the simplified diagnosis focusing exclusively on the THEN terms, which is further decomposed into contributions from dynamic and various physical processes:

$$THEN = -\frac{g}{R} p_0^{\frac{R}{c_p}} p_s^{1-\frac{R}{c_p}} \int_{z_s}^{z_t} \frac{1}{\theta^2} \left(-\vec{\boldsymbol{V}} \cdot \nabla\theta + \dot{Q}_{DIAB}\right) dz \tag{6}$$

$$\dot{Q}_{DIAB} = \dot{Q}_{CPS} + \dot{Q}_{MP} + \dot{Q}_{RA} + \dot{Q}_{BL} \tag{7}$$

where $\vec{\boldsymbol{V}}$ represents the wind velocity, $\dot{Q}_{DIAB}$ denotes the total diabatic heating produced by physical parameterization schemes including CPS, microphysics (MP), radiation (RA), and boundary layer turbulence (BL).

Figure 5 shows the azimuthal mean of SPT contributions from MP, CPS, RA, BL and total diabatic heating (DIAB) for all simulations during the rapid intensification period (18–42 h). In CTRL runs, the DIAB-induced pressure fall strengthens with increasing resolution, accompanied by an inward-moving peak center from 120 km to 60 km radius. This increasing trend is consistent with the enhancement of p_{min} shown in Figure 4. Among all physical processes, CPS and MP are the two dominant components, whereas the contributions from RA and BL are negligible. As resolution increases, the contribution from CPS gradually weakens in the inner region and is increasingly replaced by that from MP. However, at outer regions beyond 200-km radius, CPS remains the dominant component across all resolutions. This contrasting behavior underscores the distinct role of well-organized eyewall convection in the inner region versus smaller-scale convections in outer regions. The former is gradually resolved at

Accepted for publication in *Monthly Weather Review.* DOI 10.1175/MWR-D-25-0241.1.

higher resolutions, leading to a more rapid decline in CPS precipitation ratio in typhoons compared to the global mean, as shown in Figure 3. The SA-MB runs produce nearly the same radial SPT distribution as CTRL, with differences mostly within 2 hPa h^{-1}, consistent with their similar evolutions of p_{min}. On the other hand, SA-ER substantially reduces CPS contributions compared to CTRL across all resolutions except at 60 km, where both CPS and MP are enhanced. At 60 km, the enhanced mass flux induced by the increased entrainment rate outweighs its diluting effect, resulting in a net increase in CPS heating. At 30- and 15-km resolutions, the enhancement of MP more than compensates the suppression of CPS, yielding a net pressure fall maxima of about 6 hPa h^{-1} from DIAB. At 7.5- and 3.75-km resolutions, there appears a marked reduction in MP within the 60- and 120-km radius, respectively. This reduction of MP, along with continued suppression of CPS, outweighs enhanced MP contributions in outer regions, thus producing local pressure rise and weaker typhoon intensity.

Accepted for publication in *Monthly Weather Review.* DOI 10.1175/MWR-D-25-0241.1.

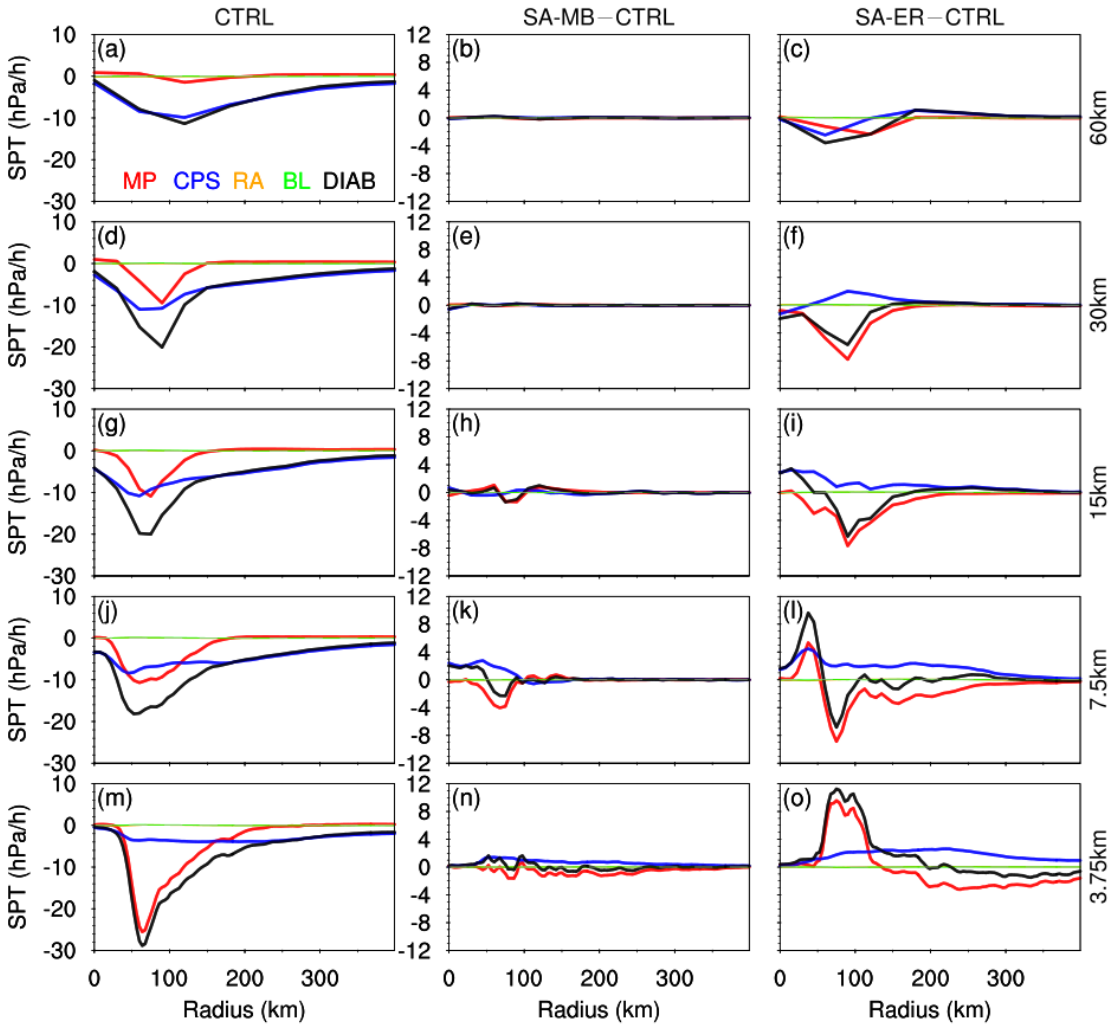


Figure 5 Azimuthally averaged surface pressure tendency (SPT, hPa h^{-1}) due to microphysics (MP), convection parameterization (CPS), radiation (RA), boundary layer turbulence (BL), and total diabatic heating (DIAB) for CTRL, along with differences compared to SA-MB and SA-ER runs at resolutions of (a–c) 60 km, (d–f) 30 km, (g–i) 15 km, (j–l) 7.5 km and (m–o) 3.75 km during 18–42 h.

In the following, we use the 15-km and 3.75-km simulations to illustrate the mechanistic impact of different scale-aware CPS on typhoons. Figure 6 displays the horizontal distribution of 18–42 h averaged total, CPS and MP precipitation for 15-km runs in CTRL, SA-MB and SA-ER experiments, overlaid with the corresponding SPT components of diabatic heating (contours). In CTRL, the total precipitation features an asymmetric eyewall with peak rainfall exceeding 500 mm d^{-1}, along with two connected rainbands: one in the southwest with rainfall around 200 mm d^{-1} and another in the northeast below 150 mm d^{-1}. The SPT generally coincides with the precipitation

Accepted for publication in *Monthly Weather Review.* DOI 10.1175/MWR-D-25-0241.1.

distribution, with a peak value of about −50 hPa h^{-1} near the precipitation center. Within a 120-km radius of the typhoon center, MP dominates the precipitation and diabatic heating, while CPS contributions prevail in outer regions. SA-MB yields precipitation and SPT nearly identical to CTRL, with the 120-km azimuthally averaged difference of less than 2% in each component, as indicated by the numbers in the panels. By contrast, SA-ER exhibits a further suppression of CPS precipitation (SPT) by 27.92 mm d^{-1} (1.89 hPa h^{-1}), accompanied by an increase in MP precipitation (SPT) of 46.25 mm d^{-1} (2.84 hPa h^{-1}). The underlying mechanism is that the microphysics takes up the convective instability that is left over by CPS (Wang and Zhang 2013). The enhancement of MP more than compensates for the reduction of CPS, yielding net increases of 18.34 mm d^{-1} in total precipitation and 0.95 hPa h^{-1} in pressure fall, which is responsible for the lowest p_{min} of SA-ER run in Figure 4h.

Accepted for publication in *Monthly Weather Review.* DOI 10.1175/MWR-D-25-0241.1.

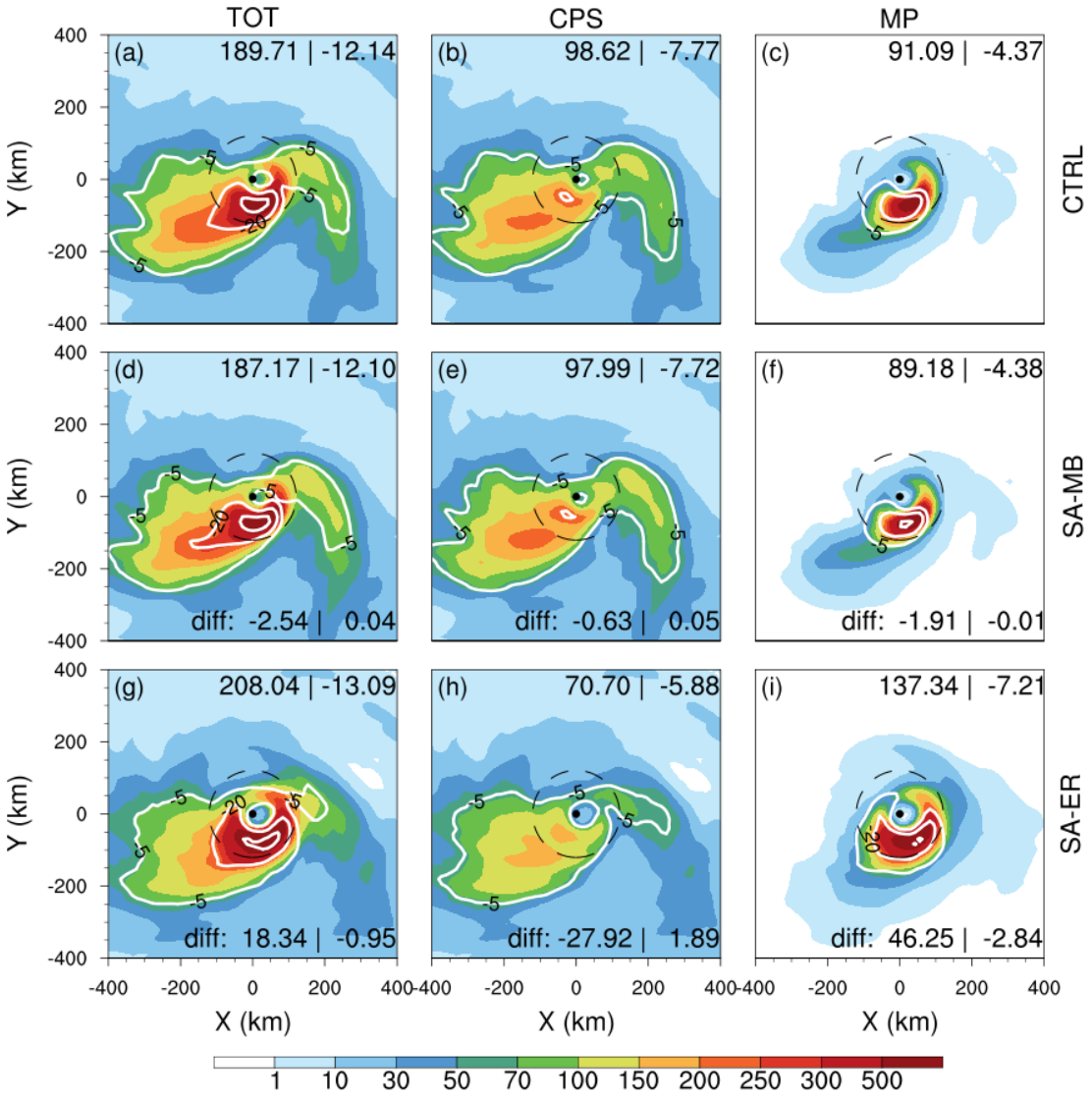
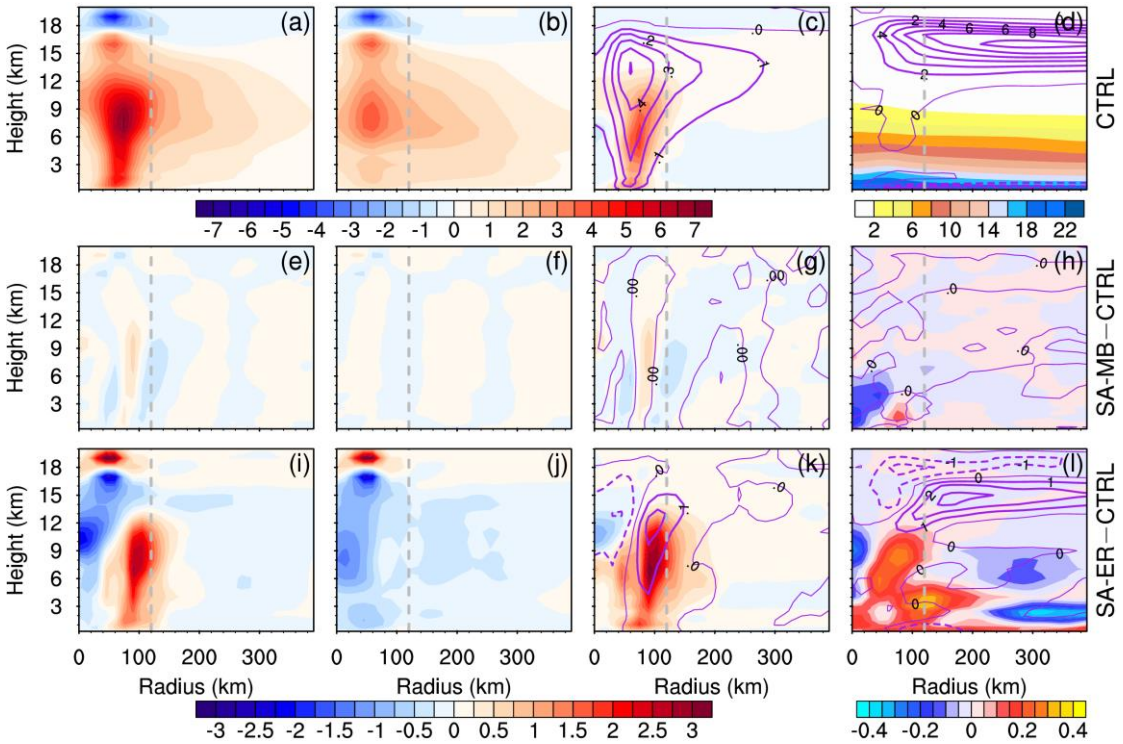


Figure 6 Simulated precipitation (shaded, mm d^{-1}) and diagnosed surface pressure tendency (SPT; contours, hPa h^{-1}) averaged over 18–42 h for CTRL, SA-MB and SA-ER runs at 15-km resolution. The azimuthally averaged precipitation (left number) and SPT (right number) within a 120-km radius are indicated in the top-right corner, along with the differences with CTRL in the bottom-right corner. Left, middle and right columns refer to total (TOT), convection parameterization (CPS) and microphysics (MP) components, respectively. Black dashed circles denote the 120-km radius, and the black dots mark the typhoon centers.

To illustrate the influence of CPS on vertical thermal and dynamical structures, Figure 7 gives the temporal and azimuthally averaged vertical profile diabatic heating, wind velocity, and specific humidity in CTRL and the differences against SA-MB and SA-ER runs. In CTRL, a wall of diabatic heating extends radially outward with height, peaking at 7 K h^{-1} near 7-km altitude (Figure 7a). CPS heating primarily contributes to

Accepted for publication in *Monthly Weather Review.* DOI 10.1175/MWR-D-25-0241.1.

the total heating in the middle and upper layers, whereas MP heating dominates in the lower and middle levels. The MP heating coincides closely with vertical velocities exceeding 0.1 m s^{-1}, and is accompanied by the low-level inflow and upper-level outflow (Figure 7d). The SA-MB simulation remains largely consistent with CTRL, with differences of CPS and MP heating only marginally observed (Figure 7f, g). By contrast, SA-ER exhibits pronounced negative anomalies in CPS heating, with maximum suppression of 3 K h^{-1} at 17-km and 1.5 K h^{-1} at 8-km. The instability left over by CPS, in conjunction with positive anomalies of grid-scale updrafts (Figure 7k) and specific humidity (Figure 7l), is then released through MP processes. As a result, SA-ER develops a positive MP heating anomaly throughout the troposphere, peaking at approximately 3 K h^{-1} around a 90 km radius, which amplifies the total diabatic heating and deepens the pressure fall. In summary, at 15-km resolution (and similarly at 30-km resolutions), SA-MB yields horizontal and vertical typhoon structures nearly identical to CTRL, due to their comparable levels of CPS suppression. SA-ER markedly suppresses parameterized eyewall convection while inducing enhanced grid-scale stratiform processes, which more than offset the CPS reduction and lead to deeper storms.



Accepted for publication in *Monthly Weather Review.* DOI 10.1175/MWR-D-25-0241.1.

Figure 7 Azimuthally averaged fields for CTRL during 18–42 h: (a) total diabatic heating, (b) convection parameterization heating, (c) microphysics heating (shaded, K h^{-1}) and vertical velocity (contours, m s^{-1}), (d) specific humidity (shaded, g kg^{-1}) and radial winds (contours, m s^{-1}). Panels (e-h) and (i-l) show the differences relative to CTRL for SA-MB and SA-ER runs, respectively. Dashed gray lines indicate the 120-km radius.

Figure 8 presents the precipitation and SPT distributions at 3.75-km resolution. The CTRL and SA-MB simulations exhibit patterns similar to those at 15 km, but with higher precipitation rates, a more contracted and symmetric eyewall, and a stronger southwestern rainband. However, in SA-ER experiment, both subgrid convection and microphysical processes are weakened within a 120 km radius, resulting in a reduction of total precipitation by 83.35 mm d^{-1} and SPT by 5.03 hPa h^{-1}. Conversely, the outer spiral rainband intensifies, with the 300 mm d^{-1} rainfall belt extending outward to 400 km, an indicator of weakening typhoon intensity (Wang 2009; Li and Wang 2012). The corresponding vertical thermal and dynamical structures are shown in Figure 9. Compared to 15-km simulations, CTRL produces a thinner eyewall with stronger diabatic heating throughout the troposphere. SA-MB run closely resembles CTRL, whereas SA-ER substantially suppresses CPS outside the 120-km radius, producing a cooling anomaly of ~1 K h^{-1} near 6 km, which is offset by a broad MP warming anomaly reaching 1.5 K h^{-1} at the same altitude. As a result, the total diabatic heating exhibits multiple positive centers in the outer spiral rainbands, stronger than those in CTRL and SA-MB (Figure 8). This enhanced heating in outer regions plays a role in impeding inward momentum and moisture convergence (Wang 2002; Chen et al. 2018), resulting in a weakened low-level inflow, a pronounced downdraft anomaly in the inner region, and a drier boundary layer (Figure 9k and 9l). Consequently, the development of eyewall is inhibited, leading to the lowest intensity among the three.

In short, scale-aware CPS exhibit distinct behaviors in typhoon simulations. The scheme that scales cloud-base mass flux (SA-MB) performs comparably to the default CPS across all resolutions, whereas the scheme that scales entrainment rate (SA-ER) generally improves typhoon simulation accuracy, with this improvement largely

Accepted for publication in *Monthly Weather Review.* DOI 10.1175/MWR-D-25-0241.1.

sustained across resolutions. The exception occurs at the finest resolution (3.75 km), where enhanced warming in the outer spiral rainbands disrupts the secondary circulation, resulting in weakened storm intensity.

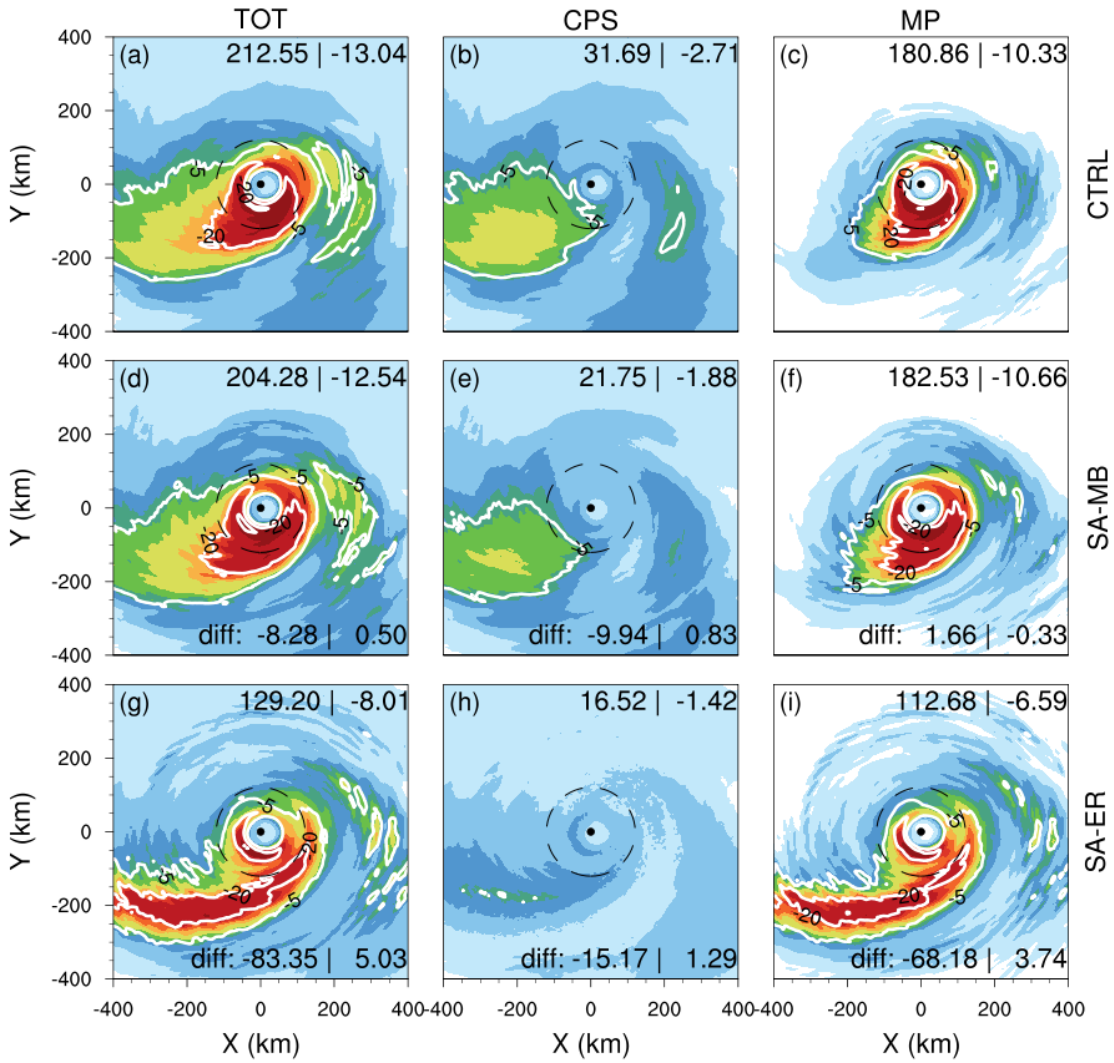


Figure 8 Same as Figure 6, but for the 3.75-km resolution simulations.

Accepted for publication in *Monthly Weather Review.* DOI 10.1175/MWR-D-25-0241.1.

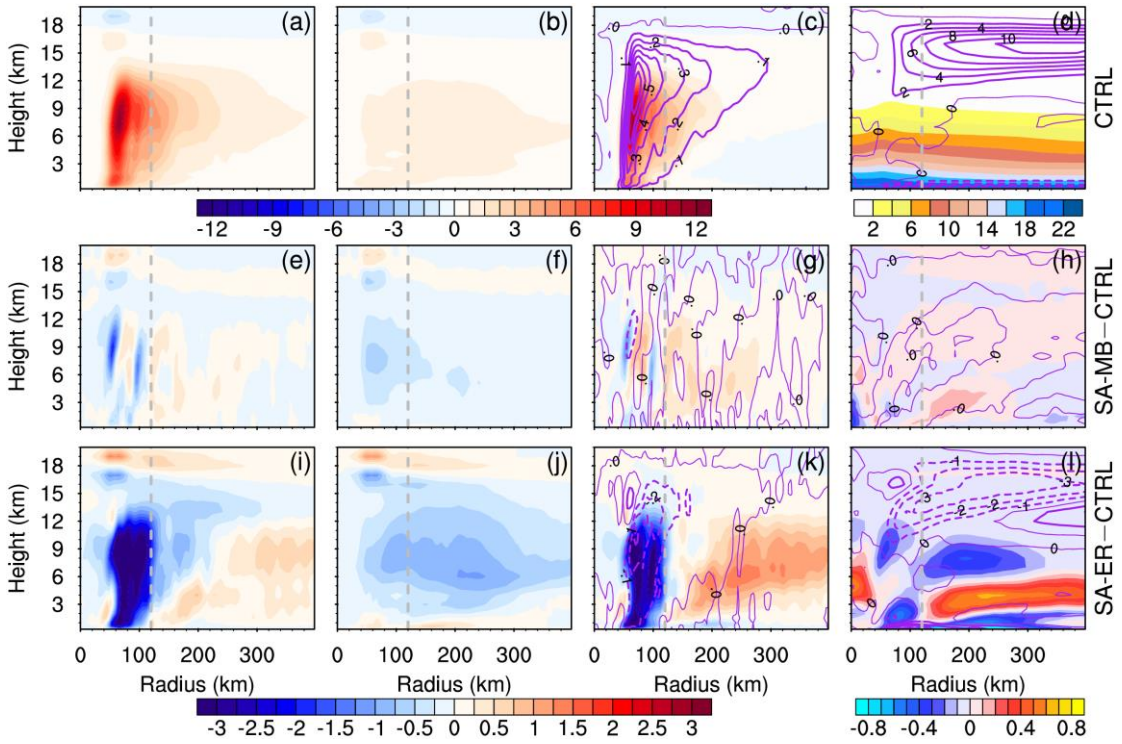


Figure 9 Same as Figure 7, but for the 3.75-km resolution simulations.

c. Comparison with explicit convection at the convection-permitting scale

To assess whether scale-aware CPS can outperform convection-permitting simulations, the explicit simulation (NOCP) at 3.75-km resolution is included for comparison in Figures 4m–4o. It shows that the simulated track in NOCP veers northward at a larger angle than observation after 30 h, leading to much greater track deviation than CPS runs after 48 h. This deviation arises because, relative to SA-ER, typhoon Krosa shifts further eastward, which in turn strengthens the WPSH between the two typhoon systems and enhances the northerly flow (Figure S4). Meanwhile, NOCP substantially underestimates the intensity in both p_{min} and v_{max} (Figure 4n and 4o).

The horizontal and vertical structures are provided in Figure 10. Compared with CTRL, NOCP produces a much weaker and more asymmetric eyewall, with heavy rainfall over 200 mm d^{-1} substantially reduced and confined to the southern sector. The 120-km averaged precipitation and surface pressure fall decreases to 127.92 mm d^{-1} and 7.51

Accepted for publication in *Monthly Weather Review.* DOI 10.1175/MWR-D-25-0241.1.

hPa h^{-1}, respectively—even weaker than SA-ER. In contrast, precipitation outside the eyewall is overactive yet less organized than in any CPS run, manifesting as fragmented rainbands. This suggests that a resolution of ~4 km remains insufficient to fully capture the fine-scale structure of typhoon (Judt et al. 2021; Wang, 2022; Majumdar et al. 2023; Polichtchouk et al. 2025). This scale mismatch prolongs the accumulation of convective instability, leading to enhanced but sporadic convective outbursts that appear as isolated cells or squall lines outside the eyewall. Such deficiencies hinder the storm's structural organization, characterized by weakened updrafts and pronounced cooling anomalies throughout the troposphere within a 120-km radius, ultimately resulting in the weakest intensity among all simulations. These findings highlight that even at the convection-permitting scale, parameterized representation of subgrid convective processes remains indispensable (Majumdar et al. 2023; Polichtchouk et al. 2025).

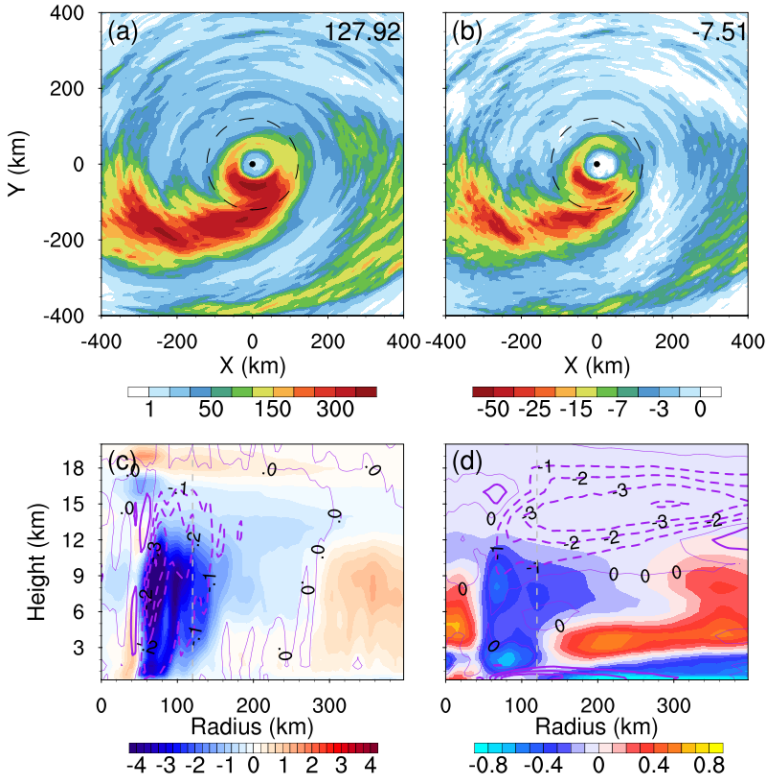


Figure 10 Horizontal and vertical structures of the explicit simulation at 3.75 km during 18–42 h: (a) Precipitation (mm d^{-1}), (b) surface pressure tendency due to total diabatic heating (hPa h^{-1}), azimuthally averaged difference with CTRL for (c) diabatic heating (shaded, K h^{-1}) and vertical velocity (contours, m s^{-1}), (d) specific humidity (shaded, g kg^{-1}) and radial winds (contours, m s^{-1}). Numbers in the top-right corner in (a, b) indicate the azimuthal mean within a 120-km radius.

Accepted for publication in *Monthly Weather Review.* DOI 10.1175/MWR-D-25-0241.1.

d. Sensitivity analysis

The scheme that most strongly suppresses parameterized convection (SA-ER) improves upon the scheme that suppresses it least (CTRL). This raises the question of whether the ability to suppress parameterized convection as resolution increases is critically important for typhoon modeling. To examine whether a higher degree of CPS precipitation suppression leads to improved typhoon simulation, we conducted a set of sensitivity experiments for Typhoon Lekima at 15-km resolution using the scale-aware cloud-base mass flux scheme (SA-MB). By tuning the parameter of convective updraft radius (R_c in Eq. 3) through extensive trial-and-error exercises, we adjusted the global CPR of SA-MB to 59.33% (SA-MB-SEN), a value even lower than that of SA-ER (61.54%). The simulated track and intensity are shown in Figure 11. Despite the stronger subgrid convection suppression, SA-MB-SEN exhibits almost identical performance to SA-MB and still performs worse than SA-ER. The underlying reason is that, although the degree of CPS precipitation suppression appears comparable, the resulting circulations, after being adjusted through atmospheric thermodynamic and dynamic feedback, are fundamentally different. As shown in Figure S5, SA-MB exhibits a distinctly more northwestward position of Typhoon Krosa compared to ERA5, with the subtropical high (5860 gpm) failing to connect between the two typhoons. Although SA-MB-SEN slightly alleviates these biases, the improvement is far less pronounced than that in the SA-ER run, particularly in terms of the southeastward shift of Krosa's position and the remarkable intensification of the subtropical high ridge. Consequently, the simulation bias in SA-MB-SEN remains substantially larger than that in SA-ER. This indicates that stronger suppression of parameterized convection does not intrinsically lead to better model performance.

Accepted for publication in *Monthly Weather Review.* DOI 10.1175/MWR-D-25-0241.1.

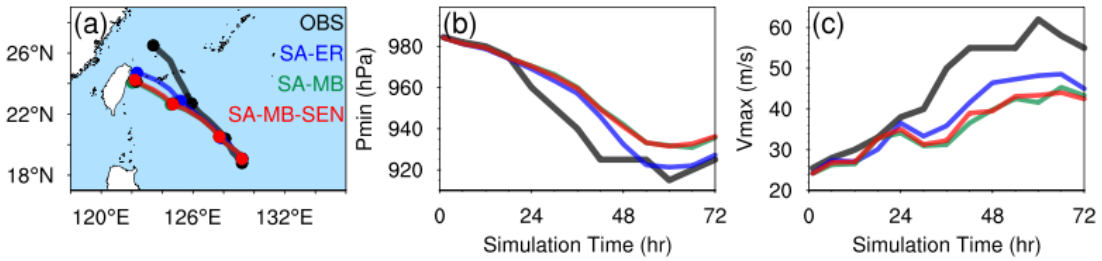


Figure 11 Observed and simulated 72-h (a) tracks, (b) minimum sea level pressure (p_{min}, hPa), and (c) maximum 10-m wind speed (v_{max}, m s^{-1}) for typhoon Lekima at 15-km resolution. Dots in (a) mark the typhoon locations at 24-h intervals. SA-MB-SEN refers to a tuning run of SA-MB with global CPR of 59.33 %.

5. Verification case: Typhoon Soudelor (2015)

In this section, simulations of super typhoon Soudelor (2015) are examined to further validate the conclusions drawn from Lekima. Figure 12 presents the observed and simulated track and intensity. All simulations capture the northwestward track reasonably well, with track errors remaining within 150 km. The error mainly accumulates from a southward deviation after 24 h, which gradually decreases as resolution increases. Among the three experiments, SA-ER produces a track closer to observations than SA-MB and CTRL, particularly at finer resolutions, where it reduces the average track error by approximately 10 km. In regrading typhoon intensity, Soudelor is stronger than Lekima, with p_{min} and v_{max} of 905 hPa and 68 m s^{-1}., compared to 915 hPa and 62 m s^{-1} in Lekima. The CTRL and SA-MB simulations systematically underestimate the peak intensity by about 35–70 hPa in p_{min} and 14–40 m s^{-1} in v_{max}. The bias is substantially alleviated in SA-ER simulations, with improvements of 10–22 hPa in p_{min} and 5–10 m s^{-1} in v_{max}. The most striking is that in this case, the intensity improvement is also manifested at 3.75 km. These results confirm the superiority of the SA-ER over the other two schemes. As for the NOCP run at 3.75-km resolution, it produces the weakest intensity among all experiments, reaffirming that the parameterized representation of subgrid convective processes

Accepted for publication in *Monthly Weather Review.* DOI 10.1175/MWR-D-25-0241.1.

remains indispensable for typhoon simulations, even at convection-permitting scales.

To understand why typhoon intensity improves at 3.75 km in SA-ER run, Figure 13 compares the horizontal and vertical structures of CTRL and SA-ER runs (SA-MB run is omitted as it closely resembles CTRL). In the CTRL run, Soudelor develops a more compact eye and a stronger eyewall than Lekima, with 120-km mean precipitation and SPT increased to 291.86 mm d^{-1} and 18.16 hPa h^{-1}, compared to 212.55 mm d^{-1} and 13.04 hPa h^{-1} in Lekima. In SA-ER run, the CPS contribution is substantially suppressed by 10.72 mm d^{-1} and 0.98 hPa h^{-1}, while microphysical processes provide excessive compensating precipitation of 43.8 mm d^{-1} and SPT of 2.88 hPa h^{-1}. Importantly, the rainfall maximum remains confined within 120 km, without the pronounced outer spiral rainbands as evident in Lekima. This configuration enhances inner-core precipitation and diabatic heating, ultimately deepening the central pressure by about 1.9 hPa h^{-1} relative to CTRL. In the vertical, SA-ER run shows pronounced MP heating anomalies concentrated within a 30-km radius, accompanied by stronger updraft anomalies, suggesting a further contraction of the eyewall. The contrasting performance between Lekima and Soudelor at 3.75 km suggests that the SA-ER approach tends to be more effective for typhoons that are more compact and intense. Zhao et al. (2024) noted that their power-law relationship has not been extensively validated across a wide range of LES cases, implying that the degree of convective suppression at high resolutions may be case-dependent. Further investigation with a broader set of cases is therefore warranted.

Accepted for publication in *Monthly Weather Review.* DOI 10.1175/MWR-D-25-0241.1.

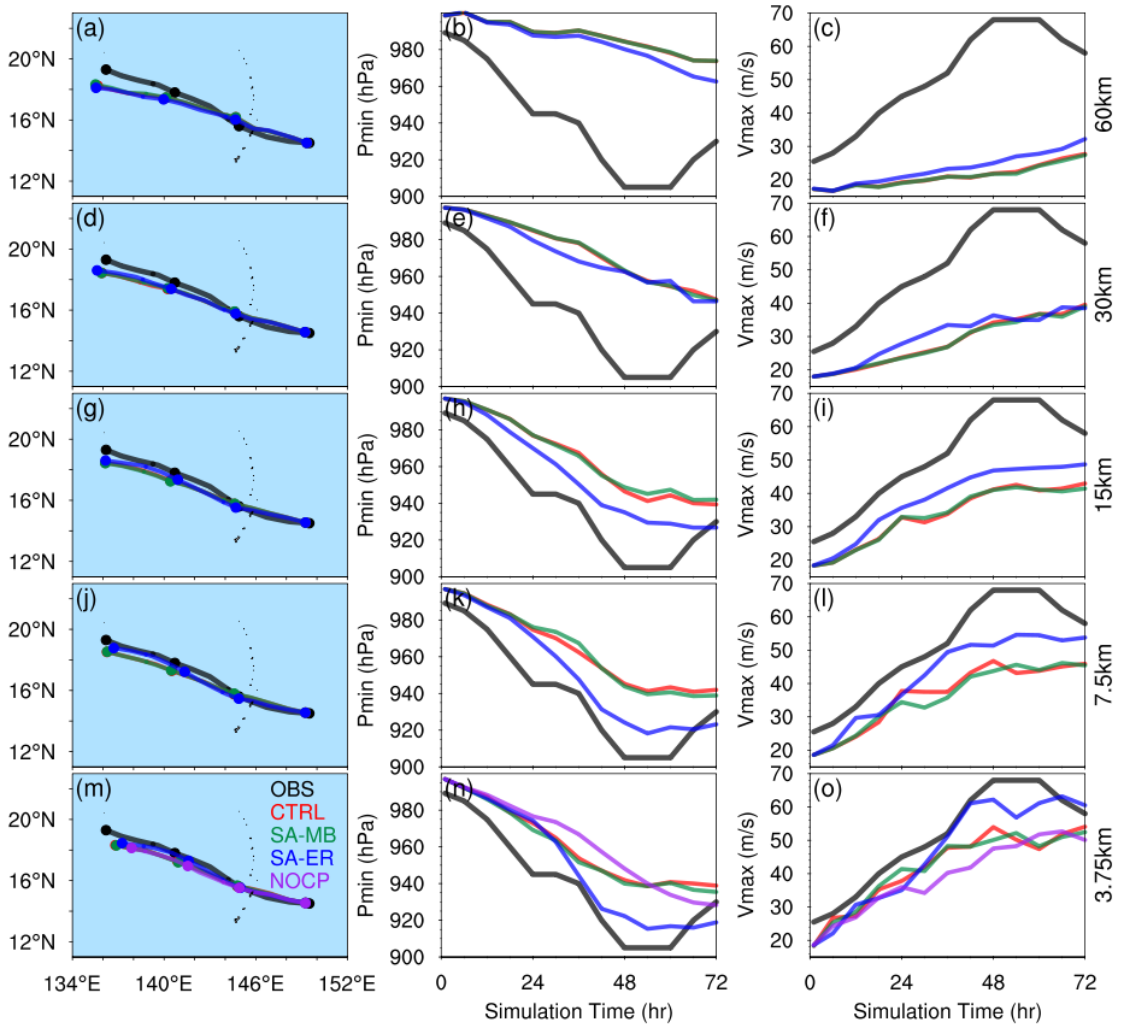


Figure 12 Same as Figure 4, but for typhoon Soudelor (2015).

Accepted for publication in *Monthly Weather Review.* DOI 10.1175/MWR-D-25-0241.1.

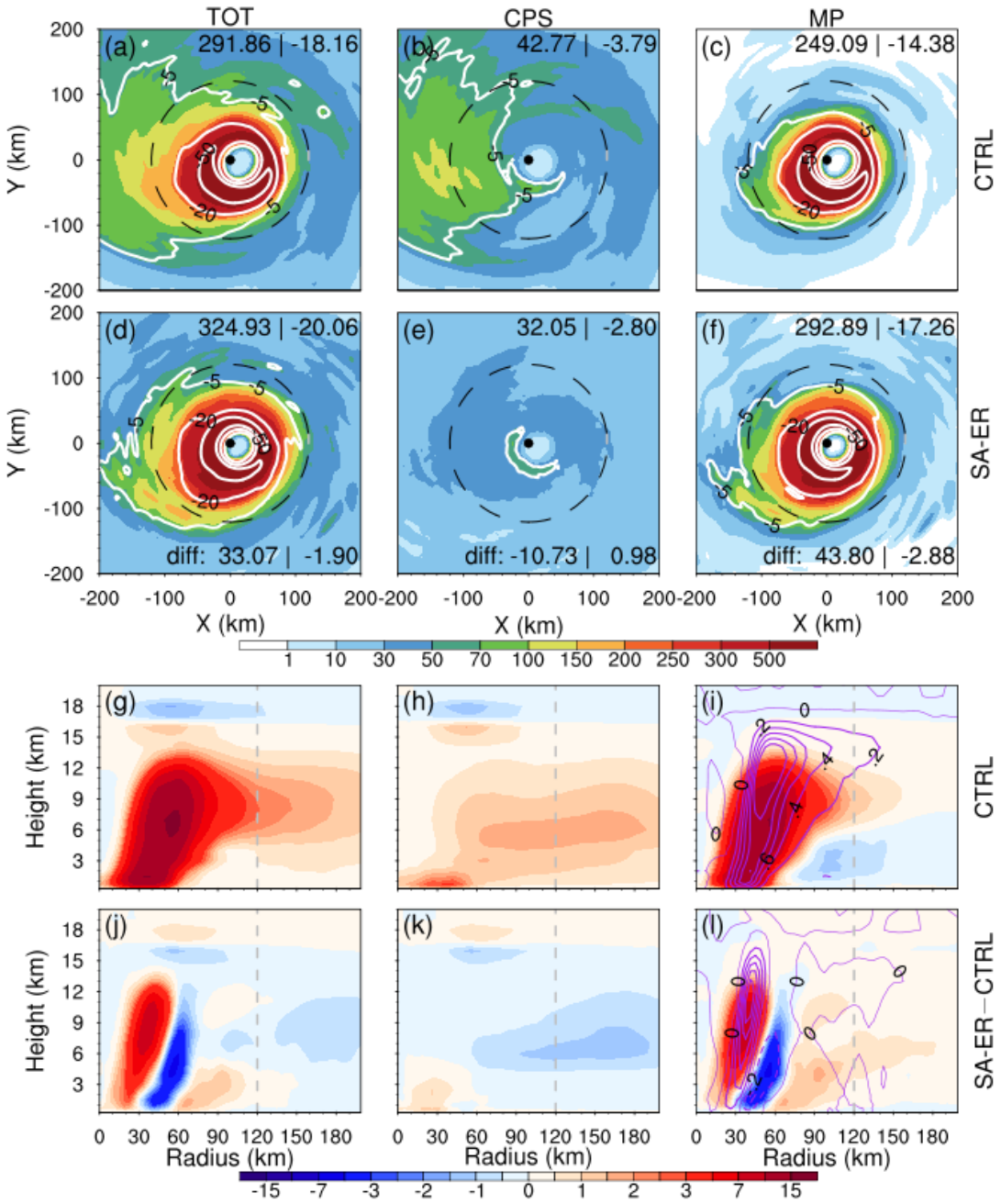


Figure 13 (a–f) Simulated precipitation (shaded, mm d^{-1}) and diagnosed surface pressure tendency (SPT; contours, hPa h^{-1}) averaged over 18–42 h for CTRL and SA-ER runs at 3.75-km resolution for Soudelor (2015). The azimuthally averaged precipitation (left number) and SPT (right number) within a 120-km radius are indicated in the top-right corner, along with the differences with CTRL in the bottom-right corner. Black dashed circles denote the 120-km radius, and the black dots mark the typhoon centers. (g–l) Corresponding azimuthal mean of diabatic heating (shaded, K h^{-1}) and vertical velocity (contours, m s^{-1}) for CTRL and differences relative to SA-ER. Dashed gray lines mark the 120-km radius. Left, middle and right columns refer to total, convection parameterization, and microphysics components, respectively.

Accepted for publication in *Monthly Weather Review.* DOI 10.1175/MWR-D-25-0241.1.

6. Conclusion and Discussion

Through a suite of global simulations with GRIST across resolutions from 60 to 3.75 km, this study systematically investigates the impacts of different scale-aware CPS on typhoon simulation based on two typhoon cases: Lekima and Soudelor. The three scale-aware implementations are: scaling convective adjustment time τ (CTRL), scaling cloud-base mass flux (SA-MB), and scaling entrainment rate (SA-ER). The key findings are summarized as follows:

All three convection schemes exhibit scale adaptivity but differ in behavior, with SA-ER demonstrating stronger CPS suppression than the other two. Globally, the ratio of CPS to total precipitation decreases with increasing resolution, from ~73% at 60 km to 57% in CTRL, 47% in SA-MB, and 40% in SA-ER at 3.75 km. This declining trend is more pronounced within typhoon systems, where the ratios drop to 45% in CTRL, 40% in SA-MB, and 22% in SA-ER at 3.75 km. Notably, CTRL and SA-MB are less effective at suppressing parameterized convection as resolution increases compared to SA-ER, which likely contributes to their weaker performance in typhoon modeling. The sharper reduction reflects the fact that highly organized convection in typhoons becomes increasingly resolved explicitly at finer resolutions.

All CPS show improved typhoon simulation with increasing resolution. Among the three schemes, CTRL and SA-MB perform comparably across all resolutions, whereas SA-ER outperforms the other two by substantially reducing systematic biases. Specifically, SA-ER reduce the mean track error by 10–45 km when compared with CTRL and SA-MB. For typhoon intensity, SA-ER mitigates the underestimation by 5–22 hPa in p_{min} and 2–10 m s^{-1} in v_{max}, equivalently 8–47% on average. While these improvements are evident across all resolutions for Soudelor, the advantage diminishes at 3.75 km for Lekima, which is less compact and intense than Soudelor.

Accepted for publication in *Monthly Weather Review.* DOI 10.1175/MWR-D-25-0241.1.

To elucidate the mechanisms by which scale-aware CPS influence typhoon intensity (p_{min}) and why SA-ER behaves differently between cases at 3.75 km, we apply the surface pressure tendency (SPT) equation to decompose contributions from individual physical processes. Results indicate that CPS and MP are the two dominant components in the SPT budget. All experiments exhibit enhanced MP and weakened CPS contributions with increasing resolution, consistent with the decreasing ratio of CPS to total precipitation. Compared to CTRL, SA-MB yields only limited improvement, as it partitions CPS and MP components similarly to CTRL, resulting in nearly identical precipitation patterns, heating structures, and thus comparable SPT and intensity evolutions. By contrast, SA-ER strengthens MP processes more vigorously, more than offsetting the CPS reduction and producing a net ~10% increase in precipitation and diabatic heating, thereby deepening the storm. However, SA-ER applied at the convection permitting scale may also trigger enhanced warming in the outer spiral rainbands, which disrupts the secondary circulation, resulting in weakened storm intensity. The contrasting performance of SA-ER between typhoons highlights a potential caveat at convection-permitting scales: it may be less effective for storms that are less compact and intense. This behavior likely originates from the power-law relationship used in SA-ER, which has not been extensively validated across a wide range of LES cases, implying that the degree of convective suppression at high resolutions may be case-dependent. Broader cases are thus warranted to better understand the sensitivity of SA-ER to scheme parameters and typhoon characteristics. While a phenomenon is observed that the scheme which most strongly suppresses parameterized convection improves upon the scheme that suppresses it least, our sensitivity analysis indicates that stronger suppression of parameterized convection does not intrinsically lead to better model performance.

At the convection-permitting scale (3.75 km), explicit convection (NOCP) produces the largest track deviation and the greatest underestimation of typhoon intensity among all simulations. Importantly, this poor performance persists regardless of storm intensity.

Accepted for publication in *Monthly Weather Review.* DOI 10.1175/MWR-D-25-0241.1.

These results underscore that, even at convection-permitting scales, parameterized representation of subgrid convective processes remains indispensable.

This study confirms that scale-aware CPS improves typhoon simulations, with the entrainment scaling approach emerging as a particularly effective pathway for enhancing typhoon intensity forecasts. These findings provide important insights for optimizing CPS in NWP models. While the two super typhoons analyzed provide distinct structural characteristics that enable a process-level evaluation of the scale-aware convection schemes, it is important to note that two cases may not represent the full spectrum of typhoon variability and the conclusions drawn from this limited sample should be viewed with caution. Moreover, as noted by Wang (2022), the behavior of scale-aware formulations may be model- and configuration-dependent, given their interactions with other physical parameterizations and the dynamical core. Future work will therefore prioritize applying these schemes across a wider range of typhoon cases and model configurations to rigorously assess their robustness and general applicability.

Acknowledgments

We thank the editor and two anonymous reviewers for their constructive comments that helped to clarify and improve the original paper. This work was jointly supported by the National Key Research and Development Program of China (2022YFF0802003), the National Natural Science Foundation of China (42575163), and the National Key Scientific and Technological Infrastructure project “Earth System Science Numerical Simulator Facility” (EarthLab). The authors declare no conflicts of interest.

Data availability statement

The ERA5 reanalysis used for model initialization were obtained from the ECMWF (https://www.ecmwf.int/en/forecasts/dataset/ecmwf-reanalysis-v5), GPM dataset is available at the NASA Goddard Earth Sciences Data and Information Services Center,

Accepted for publication in *Monthly Weather Review.* DOI 10.1175/MWR-D-25-0241.1.

see https://gpm.nasa.gov/dataaccess/downloads/gpm, and the best track data provided by the CMA Tropical Cyclone Data center are available at https://tcdata.typhoon.org.cn.

REFERENCES

Ahn, M.-S., and I.-S. Kang, 2018: A practical approach to scale-adaptive deep convection in a GCM by controlling the cumulus base mass flux. *Npj Clim. Atmospheric Sci.*, **1**, 1–8, https://doi.org/10.1038/s41612-018-0021-0.

Arakawa, A., and C.-M. Wu, 2013: A Unified Representation of Deep Moist Convection in Numerical Modeling of the Atmosphere. Part I. *J. Atmospheric Sci.*, **70**, 1977–1992, https://doi.org/10.1175/JAS-D-12-0330.1.

Bechtold, P., M. Köhler, T. Jung, F. Doblas-Reyes, M. Leutbecher, M. J. Rodwell, F. Vitart, and G. Balsamo, 2008: Advances in simulating atmospheric variability with the ECMWF model: From synoptic to decadal time-scales. *Q. J. R. Meteorol. Soc.*, **134**, 1337–1351, https://doi.org/10.1002/qj.289.

——, N. Semane, P. Lopez, J.-P. Chaboureau, A. Beljaars, and N. Bormann, 2014: Representing Equilibrium and Nonequilibrium Convection in Large-Scale Models. *J. Atmospheric Sci.*, **71**, 734–753, https://doi.org/10.1175/JAS-D-13-0163.1.

Bryan, G. H., and H. Morrison, 2012: Sensitivity of a simulated squall line to horizontal resolution and parameterization of microphysics. *Mon. Weather Rev.*, **140**, 202–225, https://doi.org/10.1175/MWR-D-11-00046.1.

Chen, G., C.-C. Wu, and Y.-H. Huang, 2018: The role of near-core convective and stratiform heating/cooling in tropical cyclone structure and intensity. *J. Atmospheric Sci.*, **75**, 297–326, https://doi.org/10.1175/JAS-D-17-0122.1.

Emanuel, K., 2018: 100 years of progress in tropical cyclone research. *Meteorol. Monogr.*, **59**, 15.1-15.68, https://doi.org/10.1175/AMSMONOGRAPHS-D-18-0016.1.

Freitas, S. R., W. M. Putman, N. P. Arnold, D. K. Adams, and G. A. Grell, 2020: Cascading toward a kilometer-scale GCM: Impacts of a scale-aware convection parameterization in the Goddard Earth Observing System GCM. *Geophys. Res. Lett.*, **47**, e2020GL087682, https://doi.org/10.1029/2020GL087682.

Gentry, M. S., and G. M. Lackmann, 2010: Sensitivity of simulated tropical cyclone structure and intensity to horizontal resolution. *Mon. Weather Rev.*, **138**, 688–704, https://doi.org/10.1175/2009MWR2976.1.

Accepted for publication in *Monthly Weather Review.* DOI 10.1175/MWR-D-25-0241.1.

Grell, G. A., and S. R. Freitas, 2014: A scale and aerosol aware stochastic convective parameterization for weather and air quality modeling. *Atmospheric Chem. Phys.*, **14**, 5233–5250, https://doi.org/10.5194/acp-14-5233-2014.

Gu, J.-F., Z.-M. Tan, and X. Qiu, 2015: Effects of vertical wind shear on inner-core thermodynamics of an idealized simulated tropical cyclone. *J. Atmospheric Sci.*, **72**, 511–530, https://doi.org/10.1175/JAS-D-14-0050.1.

Hersbach, H., and Coauthors, 2020: The ERA5 global reanalysis. *Q. J. R. Meteorol. Soc.*, **146**, 1999–2049, https://doi.org/10.1002/qj.3803.

Hong, S.-Y., and J. Dudhia, 2012: Next-generation numerical weather prediction: Bridging parameterization, explicit clouds, and large eddies. *Bull. Am. Meteorol. Soc.*, **93**, ES6–ES9, https://doi.org/10.1175/2011BAMS3224.1.

Hong, S.-Y., and J.-O. J. Lim, 2006: The WRF single-moment 6-class microphysics scheme (WSM6). *J. Korean Meteor. Soc.*, 42, 129–151.

Hong, S.-Y., Y. Noh, and J. Dudhia, 2006: A new vertical diffusion package with an explicit treatment of entrainment processes. *Mon. Weather Rev.*, **134**, 2318–2341, https://doi.org/10.1175/MWR3199.1.

Huang, C.-Y., S.-H. Sha, and H.-C. Kuo, 2022: A modeling study of typhoon lekima (2019) with the topographic influence of taiwan. *Mon. Weather Rev.*, **150**, 1993–2011, https://doi.org/10.1175/MWR-D-21-0183.1.

Huffman, G. J., E. F. Stocker, D. T. Bolvin, E. J. Nelkin, and J. Tan, 2023: GPM IMERG Final Precipitation L3 Half Hourly 0.1 degree x 0.1 degree V07. NASA Goddard Earth Sciences Data and Information Services Center, https://doi.org/10.5067/GPM/IMERG/3B-HH/07.

Iacono, M. J., J. S. Delamere, E. J. Mlawer, M. W. Shephard, S. A. Clough, and W. D. Collins, 2008: Radiative forcing by long-lived greenhouse gases: Calculations with the AER radiative transfer models. *J. Geophys. Res. Atmospheres*, **113**, https://doi.org/10.1029/2008JD009944.

Jin, H., M. S. Peng, Y. Jin, and J. D. Doyle, 2014: An evaluation of the impact of horizontal resolution on tropical cyclone predictions using COAMPS-TC. *Weather Forecast.*, **29**, 252–270, https://doi.org/10.1175/WAF-D-13-00054.1.

Judt, F., and Coauthors, 2021: Tropical cyclones in global storm-resolving models. *J. Meteorol. Soc. Jpn.*, **99**, 579–602, https://doi.org/10.2151/jmsj.2021-029.

Knippertz, P., J. Trentmann, and A. Seifert, 2009: High-resolution simulations of convective cold pools over the northwestern sahara. *J. Geophys. Res. Atmospheres*, **114**, https://doi.org/10.1029/2008JD011271.

Accepted for publication in *Monthly Weather Review.* DOI 10.1175/MWR-D-25-0241.1.

Landsea, C. W., and J. P. Cangialosi, 2018: Have we reached the limits of predictability for tropical cyclone track forecasting? *Bull. Am. Meteorol. Soc.*, **99**, 2237–2243, https://doi.org/10.1175/BAMS-D-17-0136.1.

Lei, L., Y. Ge, Z.-M. Tan, Y. Zhang, K. Chu, X. Qiu, and Q. Qian, 2022: Evaluation of a regional ensemble data assimilation system for typhoon prediction. *Adv. Atmospheric Sci.*, **39**, 1816–1832, https://doi.org/10.1007/s00376-022-1444-4.

Li, Q., and Y. Wang, 2012: Formation and quasi-periodic behavior of outer spiral rainbands in a numerically simulated tropical cyclone. *J. Atmospheric Sci.*, **69**, 997–1020, https://doi.org/10.1175/2011JAS3690.1.

——, and Y. Dai, 2020: Revisiting azimuthally asymmetric moist instability in the outer core of sheared tropical cyclones. *Mon. Weather Rev.*, **148**, 1297–1319, https://doi.org/10.1175/MWR-D-19-0004.1.

Li, X., Y. Zhang, X. Peng, W. Chu, Y. Lin, and J. Li, 2022: Improved climate simulation by using a double-plume convection scheme in a global model. *J. Geophys. Res. Atmospheres*, **127**, e2021JD036069, https://doi.org/10.1029/2021JD036069.

Lim, Y.-K., S. D. Schubert, O. Reale, M.-I. Lee, A. M. Molod, and M. J. Suarez, 2015: Sensitivity of tropical cyclones to parameterized convection in the NASA GEOS-5 model. *J. Clim.*, **28**, 551–573, https://doi.org/10.1175/JCLI-D-14-00104.1.

Liu, Y., X. Wang, Y. Liu, H. Miao, X. Zhu, W. Huang, Y. Zhao, and K. Wang, 2025: Mechanistic impacts of a scale-aware convection scheme on typhoon intensity: Diagnostics from minimum sea-level pressure. *Atmospheric Sci. Lett.*, **26**, e1315, https://doi.org/10.1002/asl.1315.

Lu, X., H. Yu, M. Ying, B. Zhao, S. Zhang, L. Lin, L. Bai, and R. Wan, 2021: Western north pacific tropical cyclone database created by the China meteorological administration. *Adv. Atmospheric Sci.*, **38**, 690–699, https://doi.org/10.1007/s00376-020-0211-7.

Majumdar, S. J., L. Magnusson, P. Bechtold, J. R. Bidlot, and J. D. Doyle, 2023: Advanced tropical cyclone prediction using the experimental global ECMWF and operational regional COAMPS-TC systems. *Mon. Weather Rev.*, **151**, 2029–2048, https://doi.org/10.1175/MWR-D-22-0236.1.

Meng, D., Z.-M. Tan, J. Li, Z. Ma, and Y. Chen, 2024: Added value of three-dimensional horizontal winds from geostationary interferometric infrared sounder for typhoon forecast in a regional NWP model. *J. Geophys. Res. Atmospheres*, **129**, e2024JD040736, https://doi.org/10.1029/2024JD040736.

Molinari, J., and M. Dudek, 1992: Parameterization of convective precipitation in

Accepted for publication in *Monthly Weather Review.* DOI 10.1175/MWR-D-25-0241.1.

mesoscale numerical models: A critical review. *Mon. Weather Rev.*, **120**, 326–344, https://doi.org/10.1175/1520-0493(1992)120<0326:POCPIM>2.0.CO;2.

Park, H., G. Kim, D.-H. Cha, E.-C. Chang, J. Kim, S.-H. Park, and D.-K. Lee, 2022: Effect of a Scale-Aware Convective Parameterization Scheme on the Simulation of Convective Cells-Related Heavy Rainfall in South Korea. *J. Adv. Model. Earth Syst.*, **14**, e2021MS002696, https://doi.org/10.1029/2021MS002696.

Park, H., J. Hwang, D.-H. Cha, M.-I. Lee, C.-K. Song, J. Kim, S.-H. Park, and D.-K. Lee, 2024: Does a Scale-Aware Convective Parameterization Scheme Improve the Simulation of Heavy Rainfall Events? *J. Geophys. Res. Atmospheres*, **129**, e2023JD039407, https://doi.org/10.1029/2023JD039407.

Peng, X., J. Fei, X. Huang, and X. Cheng, 2017: Evaluation and error analysis of official forecasts of tropical cyclones during 2005–14 over the western north pacific. Part I: Storm tracks. *Weather Forecast.*, **32**, 689–712, https://doi.org/10.1175/WAF-D-16-0043.1.

Polichtchouk, I., and Coauthors, 2025: Effects of atmosphere and ocean horizontal model resolution on tropical cyclone and upper-ocean response forecasts in four major hurricanes. *Mon. Weather Rev.*, **153**, 2257–2278, https://doi.org/10.1175/MWR-D-24-0104.1.

Rios-Berrios, R., C. A. Davis, and R. D. Torn, 2018: A hypothesis for the intensification of tropical cyclones under moderate vertical wind shear. *J. Atmospheric Sci.*, **75**, 4149–4173, https://doi.org/10.1175/JAS-D-18-0070.1.

Rogers, R. F., P. D. Reasor, and J. A. Zhang, 2015: Multiscale structure and evolution of hurricane earl (2010) during rapid intensification. *Mon. Weather Rev.*, **143**, 536–562, https://doi.org/10.1175/MWR-D-14-00175.1.

Romps, D. M., and Z. Kuang, 2010: Do undiluted convective plumes exist in the upper tropical troposphere? *J. Atmospheric Sci.*, **67**, 468–484, https://doi.org/10.1175/2009JAS3184.1.

Shi, Y., and Coauthors, 2025: Comparison of AI and NWP models in operational severe weather forecasting: A study on tropical cyclone predictions. *J. Geophys. Res. Mach. Learn. Comput.*, **2**, e2024JH000481, https://doi.org/10.1029/2024JH000481.

Song, F., and G. J. Zhang, 2018: Understanding and improving the scale dependence of trigger functions for convective parameterization using cloud-resolving model data. *J. Clim.*, **31**, 7385–7399, https://doi.org/10.1175/JCLI-D-17-0660.1.

Stevens, D. E., and C. S. Bretherton, 1999: Effects of resolution on the simulation of stratocumulus entrainment. *Q. J. R. Meteorol. Soc.*, **125**, 425–439,

Accepted for publication in *Monthly Weather Review.* DOI 10.1175/MWR-D-25-0241.1.

https://doi.org/10.1002/qj.49712555403.

Tan, Z.-M., L. Lei, Y. Wang, Y. Xu, and Y. Zhang, 2022: Typhoon track, intensity, and structure: From theory to prediction. *Adv. Atmospheric Sci.*, **39**, 1789–1799, https://doi.org/10.1007/s00376-022-2212-1.

Tiedtke, M., 1989: A comprehensive mass flux scheme for cumulus parameterization in large-scale models. *Mon. Weather Rev.*, **117**, 1779–1800, https://doi.org/10.1175/1520-0493(1989)117<1779:ACMFSF>2.0.CO;2.

Vitart, F., J. L. Anderson, J. Sirutis, and R. E. Tuleya, 2001: Sensitivity of tropical storms simulated by a general circulation model to changes in cumulus parametrization. *Q. J. R. Meteorol. Soc.*, **127**, 25–51, https://doi.org/10.1002/qj.49712757103.

Wang, W., 2022: Forecasting convection with a "scale-aware" tiedtke cumulus parameterization scheme at kilometer scales. *Weather Forecast.*, **37**, 1491–1507, https://doi.org/10.1175/WAF-D-21-0179.1.

Wang, X., and M. Zhang, 2013: An analysis of parameterization interactions and sensitivity of single-column model simulations to convection schemes in CAM4 and CAM5. *J. Geophys. Res. Atmospheres*, **118**, 8869–8880, https://doi.org/10.1002/jgrd.50690.

Wang, Y., 2002: Vortex rossby waves in a numerically simulated tropical cyclone. Part II: The role in tropical cyclone structure and intensity changes. *J. Atmospheric Sci.*, **59**, 1239–1262, https://doi.org/10.1175/1520-0469(2002)059<1239:VRWIAN>2.0.CO;2.

——, 2009: How do outer spiral rainbands affect tropical cyclone structure and intensity? *J. Atmospheric Sci.*, **66**, 1250–1273, https://doi.org/10.1175/2008JAS2737.1.

Weisman, M. L., W. C. Skamarock, and J. B. Klemp, 1997: The resolution dependence of explicitly modeled convective systems. *Mon. Weather Rev.*, **125**, 527–548, https://doi.org/10.1175/1520-0493(1997)125<0527:TRDOEM>2.0.CO;2.

Yu, H., P. Chen, Q. Li, and B. Tang, 2013: Current capability of operational numerical models in predicting tropical cyclone intensity in the western north pacific. *Bull. Am. Meteorol. Soc.*, **28**, 353–367, https://doi.org/10.1175/WAF-D-11-00100.1.

Zhang, C., and Y. Wang, 2017: Projected future changes of tropical cyclone activity over the western north and south pacific in a 20-km-mesh regional climate model. *J. Clim.*, **30**, 5923–5941, https://doi.org/10.1175/JCLI-D-16-0597.1.

Zhang, D., and Z. Ma, 2023: The generalized application of a new surface pressure

Accepted for publication in *Monthly Weather Review.* DOI 10.1175/MWR-D-25-0241.1.

tendency equation in synoptic weather systems. *J. Geophys. Res. Atmospheres*, **128**, e2023JD038580, https://doi.org/10.1029/2023JD038580.

Zhang, Y., J. Li, R. Yu, S. Zhang, Z. Liu, J. Huang, and Y. Zhou, 2019: A layer-averaged nonhydrostatic dynamical framework on an unstructured mesh for global and regional atmospheric modeling: Model description, baseline evaluation, and sensitivity exploration. *J. Adv. Model. Earth Syst.*, **11**, 1685–1714, https://doi.org/10.1029/2018MS001539.

——, R. Yu, J. Li, X. Li, X. Rong, X. Peng, and Y. Zhou, 2021: AMIP simulations of a global model for unified weather-climate forecast: Understanding precipitation characteristics and sensitivity over east asia. *J. Adv. Model. Earth Syst.*, **13**, e2021MS002592, https://doi.org/10.1029/2021MS002592.

Zhao, H., X. Yu, S. Zhang, J. Wang, Y. Gao, M. Li, L. Wu, and X. Lin, 2025: A case study of the influence of interactions between tropical cyclones and environment on binary TC tracks: Lekima and krosa (2019). *J. Geophys. Res. Atmospheres*, **130**, e2024JD042669, https://doi.org/10.1029/2024JD042669.

Zhao, Y., X. Wang, Y. Liu, and G. Wu, 2024: Are parameterized entrainment rates as scale-dependent as those estimated from cloud resolving model simulations? *Geophys. Res. Lett.*, **51**, e2024GL110735, https://doi.org/10.1029/2024GL110735.

Zheng, Y., K. Alapaty, J. A. Herwehe, A. D. D. Genio, and D. Niyogi, 2016: Improving high-resolution weather forecasts using the weather research and forecasting (WRF) model with an updated kain–fritsch scheme. *Mon. Weather Rev.*, **144**, 833–860, https://doi.org/10.1175/MWR-D-15-0005.1.

Accepted for publication in *Monthly Weather Review.* DOI 10.1175/MWR-D-25-0241.1.